DESIGN AND DEVELOPMENT OF FIBER OPTIC MEMS MICROPHONE MEASUREMENT SYSTEM

A THESIS SUBMITTED TO
THE GRADUATE SCHOOL OF NATURAL AND APPLIED SCIENCES
OF
MIDDLE EAST TECHNICAL UNIVERSITY

BY

EKIN MUHARREM KARACA

IN PARTIAL FULFILLMENT OF THE REQUIREMENTS
FOR
THE DEGREE OF MASTER OF SCIENCE
IN
ELECTRICAL AND ELECTRONIC ENGINEERING

MAY 2019

Approval of the thesis:

DESIGN AND DEVELOPMENT OF FIBER OPTIC MEMS MICROPHONE MEASUREMENT SYSTEM

submitted by **EKIN MUHARREM KARACA** in partial fulfillment of the requirements for the degree of **Master of Science in Electrical and Electronic Engineering Department, Middle East Technical University** by,

Prof. Dr. Halil Kalıpçılar
Dean, Graduate School of **Natural and Applied Sciences** _____

Prof. Dr. Tolga Çiloğlu
Head of Department, **Electrical and Electronic Eng.** _____

Prof. Dr. Barış Bayram
Supervisor, **Electrical and Electronic Eng., METU** _____

Examining Committee Members:

Prof. Dr. Nevzat Güneri Gençer
Electrical and Electronic Eng., METU _____

Prof. Dr. Barış Bayram
Electrical and Electronic Eng., METU _____

Prof. Dr. Abdullah Atalar
Electrical and Electronic Eng., Bilkent Uni. _____

Assist. Prof. Dr. Serdar Kocaman
Electrical and Electronic Eng., METU _____

Assist. Prof. Dr. Selçuk Yerci
Electrical and Electronic Eng., METU _____

Date: 21.05.2019

I hereby declare that all information in this document has been obtained and presented in accordance with academic rules and ethical conduct. I also declare that, as required by these rules and conduct, I have fully cited and referenced all material and results that are not original to this work.

Name, Surname: Ekin Muharrem KARACA

Signature:

ABSTRACT

DESIGN AND DEVELOPMENT OF FIBER OPTIC MEMS MICROPHONE MEASUREMENT SYSTEM

Karaca, Ekin Muharrem
Master of Science, Electrical and Electronic Engineering
Supervisor: Prof. Dr. Barış Bayram

May 2019, 60 pages

In this thesis, fiber optic MEMS microphone measurement system is designed and demonstrated. The displacement of the sensing element of the fiber optic microphone, the membrane, together with the optical components are 3-D modeled and simulated by means of ray tracing methods. The parameters of the optical system under different measurement conditions are optimized according to the simulation results. Based on the simulation results, the measurement system setup is designed, constructed and functionalized. The optical components of the system are chosen such that the overall system is compatible to high quality detection of the displacement of the membrane. The simulation results and experimental data are demonstrated to validate the operation of the measurement system. The system is demonstrated with optical components and the membrane, and characteristics of the fiber optic microphone are obtained. The results and observations related to the overall system are presented.

Keywords: MEMS, Fiber Optics, Interferometer

ÖZ

FİBER OPTİK MEMS MİKROFON ÖLÇÜM SİSTEMİ TASARIMI VE GELİŞTİRİLMESİ

Karaca, Ekin Muharrem
Yüksek Lisans, Elektrik ve Elektronik Mühendisliği
Tez Danışmanı: Prof. Dr. Barış Bayram

Mayıs 2019, 60 sayfa

Bu tez çalışmasında, fiber optik MEMS mikrofon ölçüm sistemi tasarlanmış ve gösterilmiştir. Zarın, fiber optik mikrofonun algılama elemanının, optik bileşenlerle birlikte yer değiştirmesi, 3-B modellenmiş ve ışın izleme yöntemleri ile benzetim yapılmıştır. Optik sistemin farklı ölçüm koşulları altındaki parametreleri benzetim sonuçlarına göre optimize edilmiştir. Benzetim sonuçlarına dayanarak, ölçüm sistemi kurulumu tasarlanmış, yapılandırılmış ve işlevselleştirilmiştir. Sistemin optik bileşenleri, genel sistemin, zarın yer değiştirmesinin yüksek kalitede saptanması ile uyumlu olacak şekilde seçilmiştir. Benzetim sonuçları ve deneysel verilerin, ölçüm sisteminin çalışmasını doğruladığı gösterilmiştir. Sistem optik bileşenler ve zar ile kurulmuş olup fiber optik mikrofonun karakteristik özellikleri elde edilmiştir. Sistemin tümü ile ilgili sonuçlar ve gözlemler sunulmuştur.

Anahtar Kelimeler: MEMS, Fiber Optik, Interferometre

To my family…

ACKNOWLEDGEMENTS

This thesis is supported by The Scientific and Technological Research Council of Turkey (TÜBİTAK) (PI: Prof.Dr. Barış Bayram, project no: **215E090**) and Middle East Technical University (BAP) (PI: Prof.Dr. Barış Bayram, project no: **BAP-03-01-2018-004**).

Firstly, I would like to express my sincere gratitude, deep kind respect and thank to Prof. Dr. Barış Bayram for his immense supervision, enlightening guidance, patience, motivation, enthusiasm and support. His dynamism, vision and sincerity has deeply enlightened me. With the wisdom he has, I have advanced myself both academically and personally. The door of his office was always open whenever I ran into a trouble spot or had a question about my research. He consistently allowed this work to be my own work, but steered me in the right the direction whenever he thought I needed it.

I would like to thank Prof. Dr. Nevzat Güneri Gencer, Assist. Prof. Dr. Selçuk Yerci Assist. Prof. Dr. Serdar Kocaman,and Prof. Dr. Abdullah Atalar for being on my thesis committee.

I want to give my special thanks to Göktuğ Cihan Özmen for being my colleague who was always there to help and support me in our last three years.

I would like to thank Yiğit Özer for his technical comments, and valuable friendship.

I would like to thank the members of ULTRAMEMS Research Group, to Asude Aydın, Eda Begüm Berberoğlu, Cansu Demirkıran, İrem Kozakçı, Mert Karamancı, Tansu Demirci, Zeynep Ayhan, İris Çelebi, İlker Oğuz, Doğa Buse Çavdır and especially to Anıl Bozyiğit, Murat Arslan and Berkay Karacaer for their technical support and useful discussions.

I would like to thank to METU TTO Director İdil Buse Kök and staff Yusuf Dudu for their helpful approach during the patent disclosure of our study. I would like to thank to METU BAP Coordinator Assoc. Prof. Dr. Hüsnü Dal and administrative staff Azize

Cabadağ Şiret, Head of METU Foreign Purchasing Directorate Mikail Yılmaz and administrative staff Mustafa Altınışık, Cihan Dalkılıç, Hayrullah Başoğlu, and METU Department of Strategy Development Director Ali Seyhan and staff Volkan Macit for their support on administrative procedures.

Finally, I want to express my deep appreciation to my family for their unconditional support and love.

TABLE OF CONTENTS

LIST OF TABLES

TABLES

LIST OF FIGURES

FIGURES

LIST OF ABBREVIATIONS

ABBREVIATIONS

MEMS:	Micro Electro Mechanical Systems
FPI:	Fabry-Perot Interferometer
FFT:	Fast Fourier Transform

CHAPTER 1

INTRODUCTION

1.1. Introduction

With the development of optical fibers, optical fibers are utilized and used in various areas such as telecommunications, medical applications, defense, avionics, sensing and measurement, seismic, imaging, etc. Unprecendented development of optical fibers is encouraged by the technological maturity supported by telecommunication sector, ease of production, durability in harsh environments and relatively low cost. The development of optical fibers is also accelerated by the academic attention drawn onto it. Academic research about them has provided the literature with low loss, low cost, high bandwidth, maturely modeled and constantly developing research area[1]. Various optical devices such as modulators, gratings, multiplexers, isolators, etc. have been realized owing to research and development of optical fibers. Besides, the research area has also led to the development of polarization maintaining, single mode, multimode, birefringent optical fibers that connect fiber optical devices together according to different properties of light.

Optical devices and optical fibers constitute optical circuits that work differently from electrical circuits. While electrical circuits generally work based on voltage, current, resistance, capacitance and inductance, optical circuits usually work based on wavelength, phase, polarization, refractive index, interference, reflection and refraction. According to electrical circuits, optical circuits provide more distinctive parameters that are measurable or observable. These distinctive parameters also enhance the abilities of the optical circuits. Although the optical circuits have different properties than electrical circuits, they also have similar trends with electrical circuits having robust and smaller systems.

Miniaturizing the systems trend is also reflected in mechanical systems [3]. Mechanical systems are shrunk with added electrical properties via MEMS (Micro Electro Mechanical Systems). MEMS has enabled the mechanical systems miniaturized from meters to micrometers. Due to their miniaturized size, these MEMS devices perform microscale and nanoscale tasks with success. The properties such as lightweight, stable performance, high resolution, low power consumption, and easy integration with other devices [2] are the key factors of the success of the MEMS devices. MEMS devices also have potential applications in RF/microwave, optical communication, energy scavenging, and bio-medical areas [4] and more. Physical sensing abilities of MEMS sensors have been highly successful and MEMS technology provided production of wide range of small, rugged and inexpensive sensing devices such as accelerometers, strain gauges, microphones, air mass flow sensors, pressure sensors and more recently gyroscopes and yaw-rate sensors [5]. Pressure sensing is one of the most effective sensing technique that MEMS devices use. It is widely used by medical, aviation, automotive industry and process control areas.

The development of pressure sensors has been highly successful so that recent devices are small, robust and they can use capacitive, piezoresistive and piezocapacitive effects. All of them are using the electrical properties of the materials. A small position change in a diaphragm or cantilever can give information about pressure change. They sense resistive or capacitive effects that have been caused by pressure change. Not only absolute pressure but also differential pressure is sensed by pressure sensors. In addition to sensing with electrical properties, the pressure change also can be detected via observation of deflection by optics.

The pressure sensors can also be used as microphones. Miniaturization process has enabled the production of macroscopic examples of them. The MEMS technology has allowed high resolution at the control of dimensions and batch production of microphones with low cost and high yield. Microphones are also defined as acoustic wave transducers operating within the audible frequency range which is stated as 20

Hz to 20 kHz. Without depending on the type of microphone, the structure of the microphone includes membrane or diaphragm and rigid anchored parts that support the membrane. The microphones have pressure equalization vents or membrane sealed under pressure to maintain the static pressure level between surrounding and inside of the microphone. Unless the pressure equalization is preserved, the diaphragm can be stuck to the bottom of back-volume or fractured under sudden pressure changes. The most commonly used micromachined microphone types are piezoelectric, piezoresistive, condenser and fiber optic microphones.

To summarize, the micromachined microphones and the distinctive properties of them are examined. Firstly, piezoelectric microphones are explained. The thin membrane which is connected to sensing bender or created from piezoelectric material constitutes the sensing part of the piezoelectric microphone. The stress caused on the membrane due to the movement creates electric voltage due to the piezoelectric effect. They do not need to be polarized because of the piezoelectric effect which gives the ability to create a voltage on themselves. One of the disadvantages of these microphones claimed is that piezoelectric microphones have the relatively high noise level than condenser microphones [6] [22].

The piezoresistive microphones basically exploit the benefits of the Wheatstone bridge. The Wheatstone bridge consists of 4 resistors; two of them are placed onto the middle of the membrane and two of them are placed onto the edge of the membrane with different polarizations. Hence, the differential resistance change is observed. Piezoresistive microphones are usually suitable for low output resistance applications [6].

The capacitive microphones which are also called as condenser microphones consist of the majority of the micromachined microphones. Usually, the diaphragm and the plate placed under the diaphragm are conductors. While they are used as electrodes, air or the material placed between them is used as a dielectric material. Generally, the dielectric material is preferred as air because the high capacitance affects the operation

speed of the microphone driving circuit. To set a reference capacitance, a DC bias voltage should be applied. The sensitivity of the capacitive microphones is dependent on the bias voltage. The increase in bias voltage causes an increase in sensitivity. Since there is a DC bias voltage limit which depends on mechanical properties of the diaphragm of the microphone, the bias voltage cannot be increased without limit [6]. If a voltage more than maximum bias voltage is applied, the diaphragm collapses. Mechanically increasing the sensitivity of the microphone is also limited. Because increasing the mechanical sensitivity of the microphone decreases the maximum bias voltage of the microphone. Since the electrical sensitivity of the microphone is dependent on the bias voltage, the decrease of the bias voltage affects the overall performance of the system. In the next section, fiber optic MEMS microphones will be given in details.

1.1.1. Fiber Optic MEMS Microphone

The fiber optic MEMS microphone is basically constructed with an optical fiber probe and the structure holding the membrane. The optical fiber probe part is responsible for transmission and receiving the light carried through the fiber. The probe part basically includes the assembly of fiber or fibers responsible for transmission and receiving, fiber connectors, a photodetector and light source. Both transmission and receiving can be provided by using only one single mode optical fiber. The structure of the microphone is the assembly of membrane covered one side with reflective material, anchors that support the membrane and elevate the membrane, and the substrate. As operational functions, detection of deflection on the membrane and producing electrical signal differentiating with membrane displacement are expected.

The fiber optic MEMS microphones are not only use different working principles than other microphones but also demonstrate better properties in various cases. Although the condenser microphones have high dynamic range and are suitable for acoustic measurement, they are not suitable for high temperature applications [7]. Besides, the frequency response of the capacitive microphones drops rapidly for the frequencies

beyond the first resonance frequency of the vibrating membrane. Because the second order Bessel function approaches to its first zero [8]. However, the frequency response of fiber optic MEMS microphones is extended beyond the second resonance frequency of the membrane which depends on the damping on the membrane [8]. Damping is controlled by the DC bias applied to the membrane. Applying DC bias controls the stress on the membrane. Hence, the higher DC bias voltage creates higher stress on the membrane. Depending on the bias voltage, the dynamic range of the microphone is adjusted. Harsh environments such as high temperature and high pressure force the design of piezoelectric and piezoresistive microphones to embrace more conservative design approach. Due to forcing factors, piezoelectric and piezoresistive microphones have limited the dynamic range [7] in comparison with capacitive microphones [21]. Additionally, piezoelectric microphones naturally have relatively high noise level [6]. Since fiber optic MEMS microphone does not need any readout or biasing circuit behind the sensor part, the fiber optic MEMS microphone is able to work in confined spaces. Also, the other microphones working with electricity have dissipation of electromagnetic radiation which affects sensitive measurement devices. Thus, the fiber optic MEMS microphone is providing an optimal solution for medical applications. The principles behind the microphone and the features of the small, robust and sensitive device are illustrated with more detail in the next section.

1.1.1.1. Working Principles of Fiber Optic MEMS Microphone

Many of MEMS fiber microphones are generally consisted of reflecting flat surface separated with the cavity and an end of the fiber. Also, the reflecting flat surface operates as a diaphragm. The diaphragm has two main functions in the fiber optic MEMS microphone configuration. First, the diaphragm operates as a transducer that converts incident acoustic energy to physical vibrations. Second, the reflective surface on the diaphragm modulates the incoming light with respect to incident acoustical waves. Various diaphragm materials such as metal-based, micromachined silicon or single/multi-mode fiber have been used depending on the application, complexity, and cost [9].

The working principle of the fiber optic MEMS microphone can be illustrated as follows. The light incident on the diaphragm is sent from the end of the fiber. The light reflects back from the diaphragm and a part of it couples to the core of the fiber. The parts that are incident on the cladding part of the fiber are not able to propagate until the photodetector and they lose their power rapidly. This phenomenon can be explained by the concept of evanescent waves. Since the incident light to the cladding cannot hold the requirements for total internal reflection, it decays by the propagation due to dissipating its power in each reflection to medium out of the cladding. The light incident to the core propagates because of holding the total internal reflection requirements. Since the light inside the core propagates with a sinusoidal pattern when total internal reflection occurs, it decays more slowly than the light incident on the cladding.

The light incident to the diaphragm and reflected from the diaphragm creates an interference pattern inside the fiber. The interference pattern is constructed by the spatial combination of at least two light sources with the same frequency or wavelength. Two phenomena can be observed when the interference occurs. These phenomena are constructive and destructive interferences. The constructive interference is defined by superpositioning of two light with the same phase which means the phase difference between two waves is even multiples of π and same frequency. In contrary, the destructive interference is defined by superpositioning of two light with the opposite phase which the phase difference between two waves is odd multiples of π and same frequency. The amplitude of the resulting light is depending on the phase difference between the interfering light. The resulting amplitude is directly proportional to the cosine of half of the phase difference. In Figure 1.1, the occurrence of interference is illustrated.

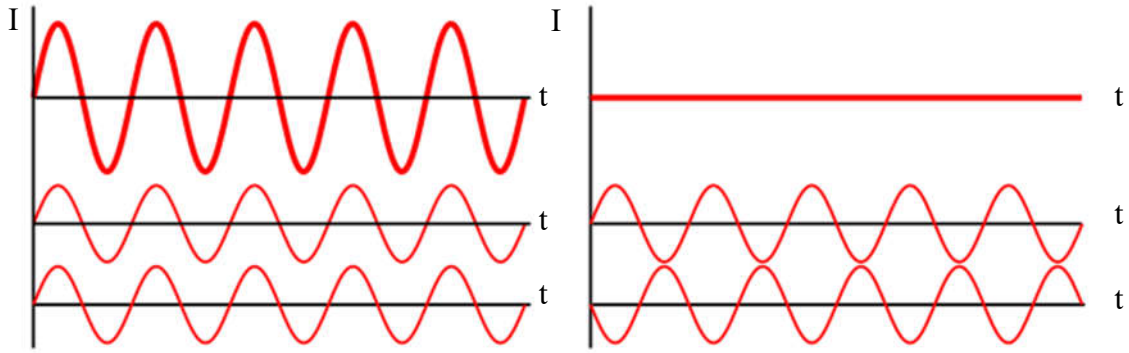

Figure 1.1. The interference of two waves. Constructive interference(left) and destructive interference(right).

With the combination of interference and the diaphragm structure mentioned above, a Fabry-Perot interferometer is built up. In the next section, the Fabry-Perot interferometer is explained in detail.

1.1.1.2. Fabry-Perot Interferometer

A Fabry-Perot Interferometer (FPI) is usually formed with two reflecting surfaces placed closely together including an optical cavity. The optical cavity can consist of air, liquids or solid material. In 1897, the Fabry-Perot Interferometer have been invented by Charles Fabry and Alfred Perot. Also, the FPI is called as etalon [1].

The interferometric structure can be constructed in two ways such as intrinsic and extrinsic FPI. In the intrinsic FPI case, two reflecting surfaces are placed into the fiber. In the extrinsic FPI case, the surfaces are separated with a different material from fiber and the cavity is formed out of the structure of the fiber. An extrinsic FPI sensor is illustrated in Figure 1.2.

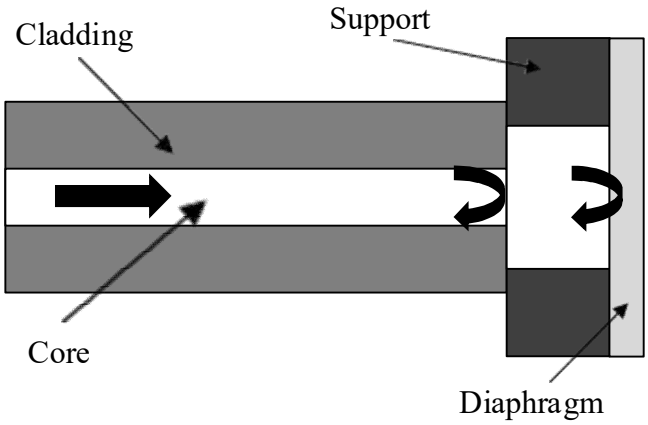

Figure 1.2. Extrinsic FPI sensor general structure

The coherent light produced propagates along the fiber and travels until the fiber end without reflection. Reflection with incidence angle 0° can be calculated with Equation 1 as shown below. In this case, n_1 represents the refractive index of the fiber core and n_2 represents the refractive index of the air since the fiber end meets with air at the end of the fiber. As a common value for core of the fiber, n_1 can be used as 1.5 and the refractive index of the air equals 1.

$$\eta = \frac{n_1}{n_2}$$
$$R = \left(\frac{\eta\cos\theta_1 - \eta\cos\theta_2}{\eta\cos\theta_1 + \eta\cos\theta_2}\right)^2, \theta_1 = \theta_2 = 0^{\circ},$$
$$= \left(\frac{n_1 - n_2}{n_1 + n_2}\right)^2 = \left(\frac{1.5 - 1}{1.5 + 1}\right)^2 = \frac{0.25}{6.25} = 4\% \quad (1)$$

Because of the reflection with incidence angle 0°, 4% of the light is reflected back from the end of the fiber. The remaining part of light travels across the cavity and reaches the reflecting face of the diaphragm. The reflected light from the diaphragm then recouples into the end of the fiber and creates interference with light reflected from fiber end. The resulting interference light intensity is formulated as in Equation 2.

$$I = 2I_d(\lambda)(1 + \gamma\cos(\varphi)) \quad (2)$$

where $I_d(\lambda)$ defines the distribution of intensity of the light source, φ is phase shift and γ is the fringe visibility of the extrinsic FPI. The phase shift is also defined by Equation 3.

$$\varphi = \frac{4\pi L}{\lambda} \tag{3}$$

where L defines the cavity length and λ defines the wavelength of the light source. The cavity length change due to the applied pressure p can be expressed as [11]

$$\Delta L = \frac{L r_o^2}{E r_o^2 - r_i^2}(1 - 2\mu)p \tag{4}$$

where E is the Young's modulus of diaphragm material, μ is the Poisson ratio, L is the cavity length, r_i and r_o are inner and outer radii of the diaphragm respectively. Equation 4 is expressing the linear change of cavity length. Since the other parameters except L and p are constant, the change of cavity length can be claimed to be linear. The linearity of the cavity length change is important for measuring the pressure change. Because measurement should be done in the linear region of the diaphragm movement. To derive meaningful data from non-linear system data, the system should be characterized thoroughly.

The interference signal created behind the Fabry-Perot cavity can be interpreted as a change between destructive and constructive interference according to the phase difference. This change can only be observed when the diaphragm reaches its own extreme maxima and minima positions. The change between destructive and constructive interference is explained by the movement of the diaphragm as much as the quarter wavelength of the light source. For example, the movement of the diaphragm between extreme points corresponds to 270 nm displacement of the center of the diaphragm for the light source operating at 1080 nm wavelength. The time between two consecutive extremes gives information about the frequency of the diaphragm movement. By counting the extreme maxima and minima points, the signal can be interpreted. The diaphragm motion is deduced from the minima and maxima

points and travel time between them gives information about the frequency of the pressure/acoustic wave applied to the membrane.

The Contributions of the Thesis

- Fiber optic MEMS microphone measurement system is designed and realized.
- The system is optimized via simulations run for 3 different topologies.
- Instead of direct access of light to the diaphragm, the light is passed through the substrate. Yet, the measurements are taken successively.
- Motorized XYZ stage is used in order to have best alignment between diaphragm of the microphone and the fiber tip.
- The chip carrier is designed and manufactured. The protection of the microphone is provided and considerably suitable measurement environment is created for the microphone.
- The measurement system is constructed with optical and electrical elements.
- The deflection of the diaphragm of the MEMS microphone is sensed and the sensitivity graph of the microphone is obtained in the audible frequency range.
- The self biasing MEMS microphone is conceptually introduced and initial measurements are taken.

CHAPTER 2

DESIGN OF THE FIBER OPTIC MEMS MICROPHONE MEASUREMENT SYSTEM

2.1. Elements of the Fiber Optic MEMS Microphone Measurement System

The fiber optic MEMS microphone transduces acoustic pressure to light variations via the reflective face of the diaphragm. The light variations are transduced into the electrical voltage signals in order to measure and quantify the data via photodetector. Hence, the measurement setup requires the use of optical and electronic circuits together. While the optical system carries the light and modulates it via the Fabry-Perot Interferometer constructed inside the MEMS microphone, the electronic system is responsible for detecting light, data acquisition, and the process of the data. Transducing points are important for the operation of the system and the data. Suitable transduction techniques and devices should be used to create a clear, concise and valid experimental environment. The system should convert one energy to another with the purpose of minimum noise and loss. In the next sections, the roles and the variety of the elements constituted to construct the system and suitability to the purpose of the system will be discussed in details. Also, the modulation techniques, which are intensity and phase modulation, used to collect data will be explained and compared with the purpose of choosing the optimum way of collecting the data. Finally, the designed simulation setup created to predict the feasibility of the measurement system will be introduced.

2.1.1. Optic Elements

2.1.1.1. Optical Fiber

As mentioned before, there are various types of fibers used to meet the different expectations of different applications. Mainly, there are 3 types of fiber; single mode,

multi mode, and microstructured optical fibers. Single mode fibers, as the name suggests, are the fibers that allow only one mode to propagate in the core of the fiber. The light is confined to relatively small space according to other fiber types. Because the diameter of the core is also a parameter of mode number allowed in the core. Besides, allowed mode number is increased when the diameter is increased [19]. The typical core diameter of single mode fiber is around 9 μm and it can change around 8.3 to 10 μm. They are less susceptible to attenuation losses and carry more data than multi mode fibers. Since they carry only one mode inside the core, they do not suffer from modal dispersion. Furthermore, the single mode fibers can be tuned to have zero dispersion at a specific wavelength in the window which is dependent on the material of the fiber.

Multi mode fibers are able to guide more than one modes in the same core. They have larger core diameter which is typically changing50, 62.5 and 100 μm than single mode fibers. The comparison of light propagation and core diameter between single mode and multi mode is illustrated in Figure 2.1. While guiding multiple modes inside the core, the light propagating inside the core is obliged to have total internal reflections. Since the propagating light loses a part of its power in each reflection, total loss due to attenuation is increased with each reflection. Thus, multi-mode fibers have higher attenuation coefficient than single mode fibers. In addition, they suffer from modal dispersion.

The dispersion can be defined as broadening of the light pulse as it propagates through the fiber. While multi mode fibers mainly suffer from chromatic and modal dispersion, single mode fibers suffer from only chromatic dispersion. Chromatic dispersion is the natural cause of the optical sources having a spectral width. As the spectral width increases, the range of the delivered wavelength increases. Since the light with different wavelength travels at a different speed in the medium, they reach the fiber end at slightly different times. Hence, pulse broadening occurs. In modal dispersion case, different modes have travels at different propagation vectors which causes reflections at different angles inside the core. The optical path increases due to the

increase in the incidence angle. The modes which have lower incidence angles reflect more according to the modes which have higher incidence angle. The number of reflections are correlated with the optical of the light. Thus, different optical path lengths of the modes cause the modes reaching in different times at the fiber end.

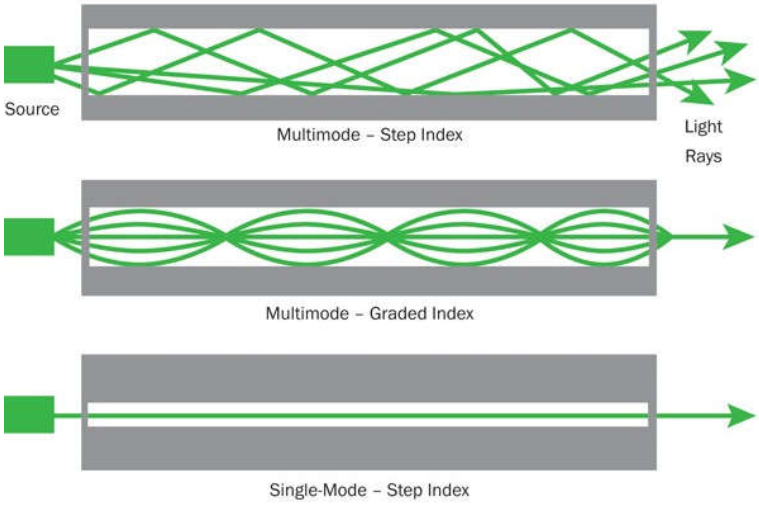

Figure 2.1. Cross sections of multi mode and single mode fibers [15]

Besides the single mode and multi mode fibers, lensed fibers are produced in order to provide higher coupling efficiency according to non-lensed fibers. Lensed fibers differ from common fiber with their specialized tips. They are produced with comprehensive properties with single mode, multi mode with different core diameters and similar range of operating wavelength. They have typically 400 nm to 1700 nm operation wavelength [24]. They have specialized tips for application specific. Conical, spherical, ball, wedge-chisel, angled and perpendicular lensed fiber tips can be shown as example for variety of the lensed fibers. Various types of lensed fibers are shown in the Figure 2.2. They can be produced with elastic polishing plate method [25], grinding, polishing [26], surface micromachining, Ar ion-beam etching technique and photoresist reflow method [27].

Lensed fibers greatly increase the power coupling ratio compared to single mode fibers [28] [29]. The power coupling efficiency between GaAs injection lasers and single mode fibers have increased from 8% for a fiber without a lens to 23% and for

a fiber with a spherical lens and 34% with a cylindrical lens [28]. While the power coupling ratio of the contact single mode fiber is 50%, the lensed fiber with working distance of 120 µm has 85% of power coupling ratio.

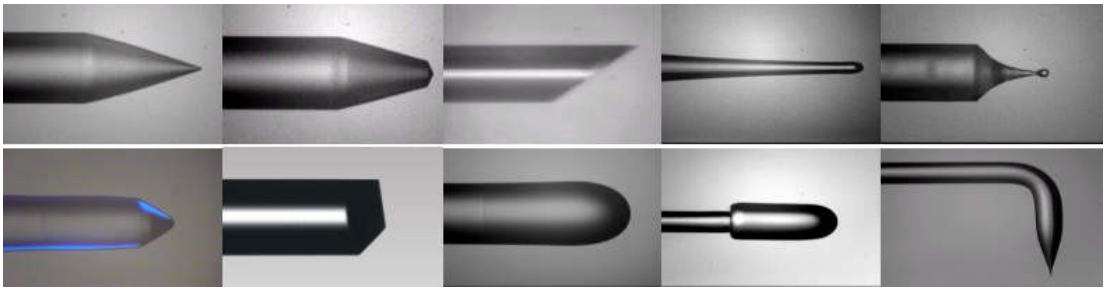

Figure 2.2 Various types of lensed fibers [34]

Comparing the single mode and multi mode fibers for the fiber optic MEMS microphone measurement system, single mode fiber is a more convenient choice because of introducing low attenuation loss and dispersion. The laser source should be used because the Fabry Perot Interferometer requires a coherent light source. The light sent through the fiber travels to the diaphragm, reflects from it and recouples to the fiber core again. Thus, minimum dispersion is beneficial for the system. Furthermore, the single mode fiber prevents the occurrence of any other modes that can affect the interference of the returned and reflected light. Because the significant amount of light is lost during reflection and light recoupling the fiber, preserving the optical power as much as possible is important for the system. Although lensed fibers have superior power coupling efficiency compared to multimode and single mode fibers, they cost 75 times more than multimode and single mode fibers cost [30] [31]. Hence, single mode fiber is decided to be used in the system.

2.1.1.2. Circulator

The optical circulator is a non-reciprocal 3 or 4 port optical element that directs the light entering a port to the consecutive port. To illustrate, the light entering port 1 is emitted from port 2 as shown in Figure 2.3 and this is valid for other consecutive ports. However, the reflected light from port 2 is redirected to port 3. Usually, the last port

does not circulate to port 1 since port 1 is generally used for light sources such as laser and operation of the laser is negatively affected by any spurious light sources reaching to the laser. Due to their relatively high isolation [20] and low insertion loss [14], they are used in fiber optic sensor applications and communication systems.

After the light entering from Port 1, it is split into two separated orthogonal polarized rays. The light is refracted in two separated rays while passing through the birefringent walk-off block A. The refracted part of the incoming light is transferred to another optical pathway. Both rays are passed through phase retardation plate and Faraday rotator as shown in Figure 2.3. While the lights are passed through the Faraday rotator, the polarization of both is rotated 90°. Then, both rays are combined in the birefringent walk-off block B and recombined light is emitted through the Port 2.

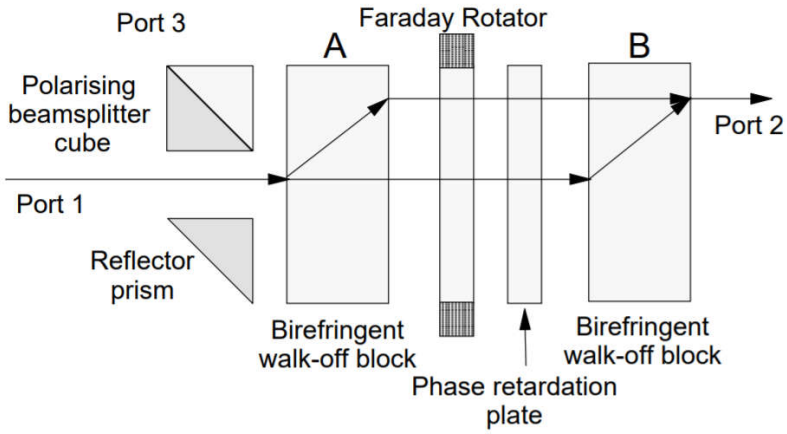

Figure 2.3. Operation of circulator from Port 1 to Port 2 [14]

In the , circulator operation from Port 2 to Port 3 is illustrated. The light entering from Port 2 is split in block B by refraction of the light into two orthogonal polarized rays again. However, the polarization of the rays traveling in the opposite direction according to the case shown in Figure 2.3. is not changed while passing through the Faraday rotator. The refracted part of the incoming light is refracted again by the block A. Then, both rays are recombined via the reflector prism and polarizing beam splitter cube. The operation of the circulator defined above is used with the purpose of

directing the light produced from the laser source to the MEMS microphone and collecting reflected light from the diaphragm. The reflected light should be collected from another fiber end in order to take measurements without affecting the light source. Since the light reflected from the fiber end and the diaphragm of the MEMS microphone is affected by the same polarization changes, property of polarization change of the circulator does not conflict with about purpose of the experiment.

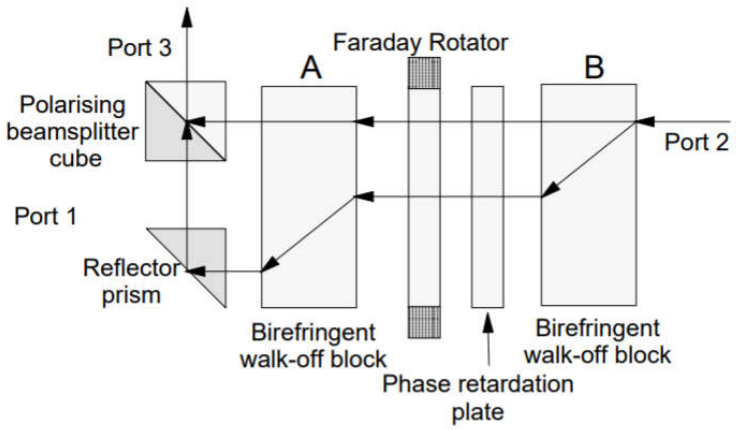

Figure 2.4. Operation of circulator from Port 2 to Port 3 [14]

2.1.2. Optoelectronic Elements

2.1.2.1. Photodetector

The photodetector is an optoelectronic device that works with the photon-matter interaction that is caused by photons with enough energy which causes the current by hitting the surface of the sensor part of the photodetector. Generally, there are two types of photodetectors: photoconductive and photodiode. The conductivity of the photoconductive type is changed by the incident flux of light. As the light flux increases, the conductivity of the device increases. The photodiode type is generally reverse biased. As a consequence of applying reverse bias, the depletion region is created. The depletion region prevents the transition of the current through the diode. The electron-hole pairs are created in the photodetector via the incident photons with

adequate energy. The incident photons with adequate energy moves an electron from the valence band to the conduction band. The produced carriers are swept from the junction by the built-in electric field of the depletion region. Hence, holes start to travel to the anode of the photodiode and electrons start to travel to the cathode of the photodiode. By the transition of the charges, the photocurrent is generated.

There are various parameters that define performance characteristics of the photodetectors. Quantum efficiency is the ratio of the number of electrons that turned into the current and the incident number of photons. It does not totally define the efficiency of the whole photodetector but it gives information about the efficiency of the sensing part of the photodetector. The responsivity is the produced current per voltage applied to the photodetector. Responsivity does not cover the whole figures of merits of the photodetector. To compare thoroughly, the detectivity value should be calculated. The detectivity value has importance when the photodiodes are especially assessed for thermal imaging applications. However, the responsivity value has higher importance than the detectivity value for our measurement system since the background related noises are insignificant for this application. The dark current is defined by the current passing through the photodiode which is not exposed to the light. It directly affects the signal to noise ratio and the quality of the photodetector. The response time is basically defined as the relaxation time between the charges produced. If the response time increases, it takes a longer time to minority carriers reach the charge neutral part of the photodiode and be recombined. Thus, recombination time increases and the increase in the recombination time after a limit causes the saturation of the photodiode. Hence, the detection of changes in the incident light is slowed down and limited.

When the photodetector materials are compared for the wavelength that can be relatively easily produced by common laser sources, Ge and InGaAs have higher responsivity among the other photodetector materials [12]. In the Figure 2.5, the responsivity graph of the commercial photodetectors is shown. Both InGaAs and Ge have responsivity around 0.85 A/W at 1550 nm. However, InGaAs detectors have

slightly better bandwidth than Ge detectors [13]. Although Ge detectors exhibit more dark current than InGaAs detectors, dark current is not vital for the application. Ge detectors exhibit hundreds of picoamperes dark current [13]. When the cost of the photodetectors is taken into account, Ge detector is chosen for the measurement system.

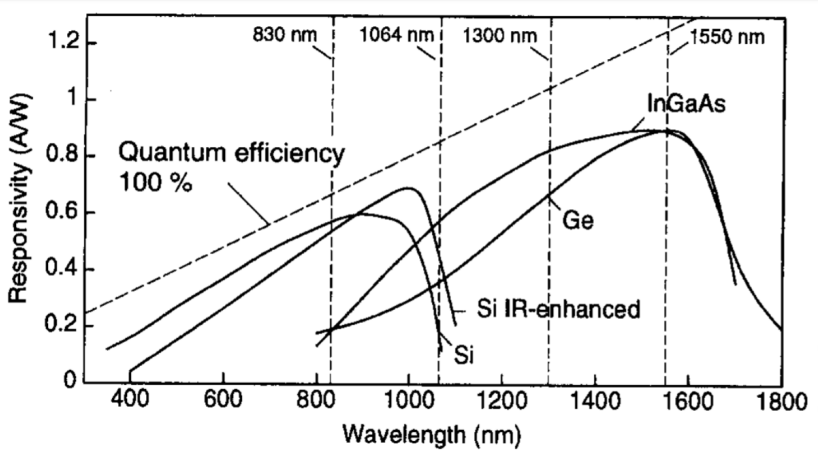

Figure 2.5. Responsivity graph of commercial photodetectors [12]

2.1.3. Electronic Elements

2.1.3.1. Data Acquisition System

Data acquisition is defined as collecting, sampling and storing the data provided by the measurements of a system related to the real world. Data acquisition systems basically convert analog data collected from a sensor or sensors to digital data and create a platform to facilitate the manipulation of the collected data. A data acquisition system consists of sensors, signal conditioning hardware, data acquisition hardware and a computer that facilitates the data acquisition software. Data acquisition hardware is responsible for digitizing the analog data, interfacing with computer via universal data transfer protocols such as PCI eX, Ethernet and USB. The interfaces are constructed with different bandwidth and different number of data lines according to the requirements of the application. Besides, the software part of data acquisition system is also specialized for manipulating, illustrating, running complex algorithms

and calculations on the collected data. The algorithms and calculations are also optimized in order to provide real time output.

Our measurement system requires a data acquisition system that can manifest specialized functions for examining the collected data. The functions can be exemplified as Fast Fourier Transform (FFT), histogram, spectrogram, and 3-D surface plot which is constituted by time, amplitude and frequency axes together in one plot. By the data acquisition system with the capabilities mentioned above, measurements are taken and characterization process is done.

2.1.3.2. Speaker and Calibration Microphone

The speaker is included in the measurement system with the purpose of generating test tones in the experiment environment. The calibration microphone is a microphone that has precise response characterized with the purpose of taking scientific measurement. By means of characterization, the multiple sensitivity graphs which are given in Volts per Pascal are provided with the microphone. The reason for the multiple graphs are given is dependency of the sensitivity of the microphone to the environmental conditions. Hence, two graphs according to free and pressured field are provided with various frequency spectrum of the microphone. The distance between the speaker and the calibration microphone should be characterized and measured in order to derive information from response graphs of the calibration microphone.

The steps of calibration of the MEMS microphone with the help of the speaker and the calibration microphone are explained. Firstly, the speaker and the calibration microphone are placed to the defined distance. The distance is approximately set in accordance with the estimated position of the MEMS microphone. Secondly, various test tones are applied via speaker and the output of the calibration microphone is observed. The pressure applied via the speaker is derived with the characterization sheet supplied with the calibration microphone. Then, the MEMS microphone is placed according to the derived pressure. The response acquired from the MEMS

microphone is converted to pressure value. Hence, the pressure vs. frequency and sensitivity vs. pressure graphs are derived.

2.2. Construction of Simulation Setup

For simulation purposes, TracePro software is used. TracePro is based on ray optics algorithms. It also supports Monte Carlo ray tracing. Besides, creating 3-D models, various analysis methods and optimization tools are provided with the software. Hence, TracePro is used as the simulation tool for the thesis.

First of all, the MEMS microphone is modeled with layer by layer structure which is consisted of diaphragm, supports and substrate. The porous structure on the diaphragm is demonstrated with the equally spaced holes perforated on the flat surface. Si and SiO_2 layers with different thicknesses are combined with their material properties defined according to the central wavelength of the laser source. The Si and SiO_2 layers are constructed such that they support the diaphragm from its outer parts and circle that is the same size with the diaphragm is subtracted from the center part of the layers. In the final configuration of the MEMS microphone, the top layer of the microphone is the diaphragm. The Si and SiO_2 layers are placed under the diaphragm. Finally, the Si substrate creates basis for the structures as it is defining the bottom layer of the whole structure.

In addition, the optical fiber carrying and collecting light is modeled in the single mode fiber configuration. The core diameter of the fiber is defined as 9 μm and the cladding diameter of the fiber is defined as 125 μm. The laser source is simulated as a light source placed into the core of the fiber. The light source is not modeled as an ideal source because the reflections and refractions are expected to occur in practical conditions. Simulating the reflections inside the fiber are predicted to evaluate the portion of the light passed on the cladding. In addition, simulating the refractions are expected to provide information about the distribution of the light on the diaphragm. The relation between optical fiber distance to diaphragm and the area covered with light on the diaphragm is anticipated. Due to refraction, a positive correlation between

the incident light and the distance of the fiber end within the area covered is expected. The distance is created basically by the substrate thickness and the spacing contributed by the supports. The basic simulation model is shown in Figure 2.6. In Figure 2.6, the surface that is placed for collecting the flux returning to the fiber is shown as (a). The single mode fiber is modeled with 9 µm core diameter and 125 µm cladding and shown as (b). 3-D modeled MEMS microphone is shown as (c). The surface shown as (d) is used for collecting the flux is escaped from the MEMS microphone.

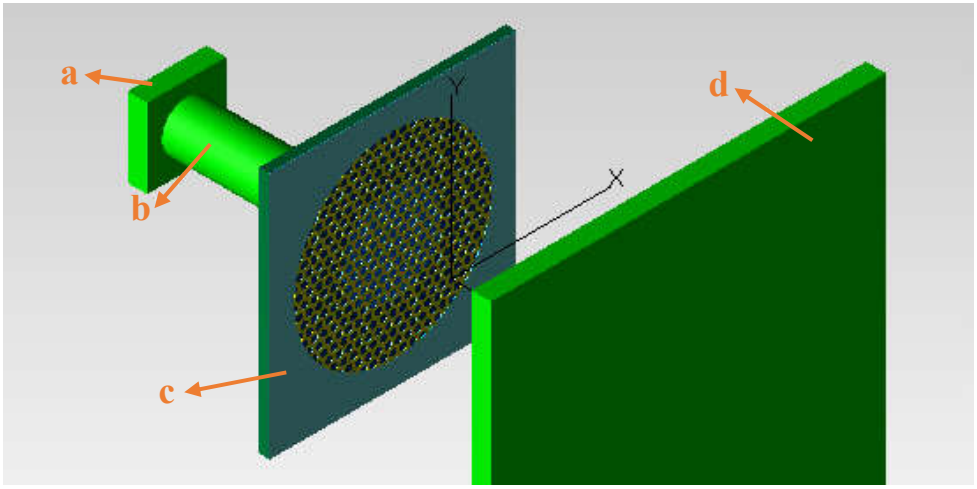

Figure 2.6. The simulation model of the MEMS microphone

In order to explain the simulation setup, the square green that is placed behind the cylinder is a surface created for measuring the returned light that is reflected from fiber end and the diaphragm itself. The cylinder represents the fiber that reaches to the substrate of the MEMS microphone. The right most square is placed with the purpose of measuring the power and density of the light that is passed from diaphragm and reached to the outer world. In the expanded perspective, the light source is placed in front of the surface to measure the returned light density and power. It is directed to the diaphragm and the light produced via the source travels inside the core of the fiber. Then, the light passes through the substrate and reaches to the diaphragm. A portion of the light reflected back to the substrate and the rest of it continues to travel to the bigger surface. Absorptions due to the materials also are covered in the simulations.

The different topologies are also covered in the Chapter 3. The topologies are created in order to examine the effects the variation of the distance of the optical fiber to the substrate, substrate thickness and the measurability of the equivalent substrate thickness.

CHAPTER 3

OPTIMIZATION OF THE MEASUREMENT SYSTEM

In this chapter, the simulation results are derived and examined. These simulations are run with the purpose of optimization of the sending and collecting the light are derived and examined. The physical parameters of the MEMS microphone are used for 3-D modeling of the microphone. The simulations and 3-D model of the microphone are done in the platform of TracePro software. TracePro software combines Monte Carlo ray tracing, analysis, CAD import/export, and optimization methods with a complete and robust macro language to solve a wide variety of new problems in illumination design [23]. TracePro is also a powerful tool for the analysis of multiple aspects of imaging systems, including stray light and polarization effects. Bulk properties including absorption, scattering, and fluorescence enable the design and analysis of devices for a wide variety of applications [23]. The results obtained in this chapter have improved the measurements of the system. The simulations are done in 3 different setups. The first setup is constructed to conceptualize the effect of the substrate thickness. The second simulation setup is formed with the purpose of defining optimum distance between fiber end to the substrate. Finally, the third setup is organized to verify the "equivalent distance" concept which is explained in detail in Section 3.4.

3.1. 3-D Model of the MEMS Microphone

In Table 3.1, the physical parameters of the MEMS microphone are given. The MEMS microphone is modeled according to the parameters given in Table 3.1. Top view of the 3-D modeled MEMS microphone is shown in Figure 3.1

Table 3.1. *Physical parameters of the MEMS microphone used in the simulation*

Dimension parameter	Value

Membrane diameter ($d_{MEMBRANE}$), µm	1000
Support length ($d_{SUPPORT}$), µm	150
Hole-to-hole diameter ($d_{HOLE\text{-}TO\text{-}HOLE}$), µm	50
Hole diameter (d_{HOLE}), µm	36
Metal thickness (t_{METAL}), µm	0.51
POLY2 thickness (t_{POLY2}), µm	1.5
POLY1 thickness (t_{POLY1}), µm	2.0
POLY0 thickness (t_{POLY0}), µm	0.51
SiN thickness (t_{SiN}), µm	0.61
Substrate thickness (t_{SUBS}), µm	>650

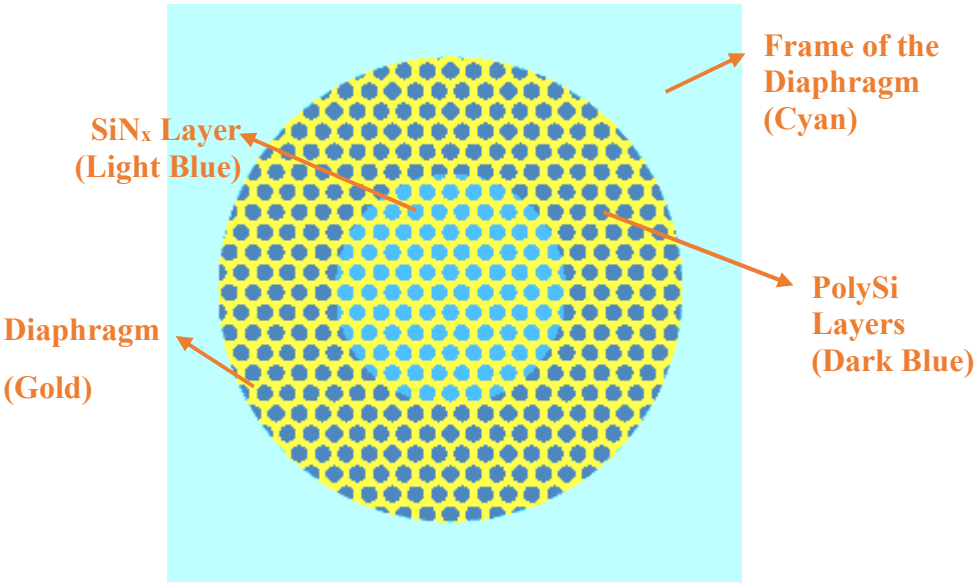

Figure 3.1. Top view of the 3-D modeled MEMS microphone

Figure 3.2. Layers of the MEMS microphone

Figure 3.2. shows the layers of the MEMS microphone. The layers are described respectively from left to right as fiber, substrate, SiN_x, POLY0, POLY1, POLY2 and Gold. Since the fiber and substrate layers are thicker than other layers, it is hard to comprehend the thickness of the other layers. Therefore, the thickness of the substrate is minimized within the scope of the simulation. The model is zoomed and placed onto YZ axis in order to demonstrate the layers more clearly. The figure is zoomed for 50 µm substrate thickness in order to show the size of the layers respective to each other. Because of the substrate layer having the thickest layer within the MEMS microphone, the effect of the thickness of the substrate is examined as a first step.

3.2. Effects of the Substrate Thickness

In the created simulation setup, the light beam is sent behind the MEMS microphone. The light beam pass through substrate, polysilicon, SiN_x and metal layer of the MEMS microphone respectively. Then, the light beam reflects back from the metal layer and travels back until the end of the fiber. Figure 3.3 shows the simulation model created for observing the effects of the substrate to the light beam. The higher density of the collected light is desired for the measurement system. Hence, it enables the collection of more convenient and detailed data. As the distance traveled in the substrate increases, the light beam is exposed to scattering and diffraction more and more. Since the SiN_x and Polysilicon layers are sub-micron thick layers, their effect on the absorption and the scattering of the light beam is not significant when compared to the effect of the substrate layer. For this reason, simulations are made by using the

TracePro software as the thickness of the substrate is variable. The thinning of the substrate by the grinder is also considered. The substrate layer thickness changed between 50 µm and 500 µm in 50 µm steps and the fiber tip is placed to the back surface of the substrate.

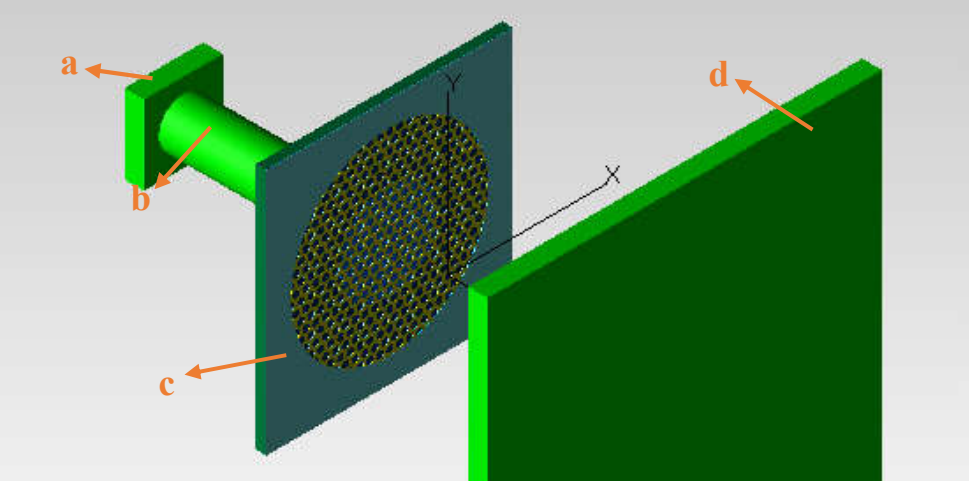

Figure 3.3. The simulation setup created to observe the effects of the substrate thickness on power ratio

In Figure 3.3, the surface that is placed for collecting the flux returning to the fiber is shown as (a). The single mode fiber is modeled with 9 µm core diameter and 125 µm cladding and shown as (b). 3-D modeled MEMS microphone is shown as (c). The surface shown as (d) is used for collecting the flux is escaped from the MEMS microphone. The layer details of the MEMS microphone are not shown in order to present the whole setup. Since the thickness of the SiN_x and Polysilicon layers are sub-micron, the details of the layer structure cannot be shown.

The power ratio which is defined as the ratio of received power obtained from fiber tip connected to the photodetector and input power pumped can be shown with the Equation 5.

$$Power\ Ratio\ (\%) = \frac{P_{received}}{P_{input}} * 100 \qquad (5)$$

In Figure 3.4, variation of the power ratio according to the change of the substrate thickness is given. Substrate thickness of 500 µm to 250 µm does not show significant change in point of power ratio. The slight variation between the range of 500 µm and 250 µm is due to the attenuation stems from the material of the substrate. As the substrate thickness decreases from 250 µm to 50 µm, the power ratio follows an exponential trend. The exponential trend is explained by the increase in the probability of collection of the reflected light beams. The distance between the diaphragm and the fiber tip decreases while substrate thickness decreases. Hence, the incidence of the light beams which come out from the fiber tip on the diaphragm are more centered according to the 500 µm substrate thickness case and the reflected beams are less diverged from the central axis. Thus, the increase in the power ratio is expected. Although the substrate thickness varies between 350 µm and 500 µm, the power ratio does not significantly change. Exponential trend is also expected in 350 and 500 µm. This phenomenon is caused by the reflection from the back surface of the substrate. 15.03% of the input power is reflected back to the end of the fiber.

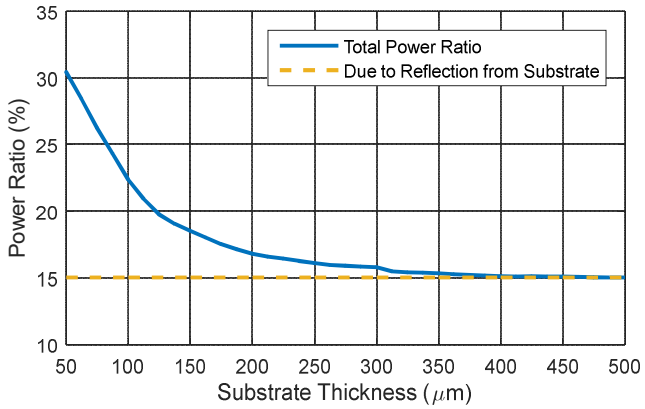

Figure 3.4. Substrate thickness vs. power ratio

3.3. Optimum Distance of Fiber End to Substrate

In Figure 3.5, the setup created for defining the optimum distance to the substrate is demonstrated. The distance between the fiber tip and substrate is variable during the simulation. The simulations are run for substrate thickness of 50 µm and 500 µm. The variation of the power ratio between substrate thickness of 50 µm and 500 µm is

expected to have a similar trend that have been shown in Figure 3.4. Distance between substrate and fiber tip is changed from 0 µm to 200 µm by the steps of 1 µm and from 200 µm to 1 mm by the steps of 25 µm.

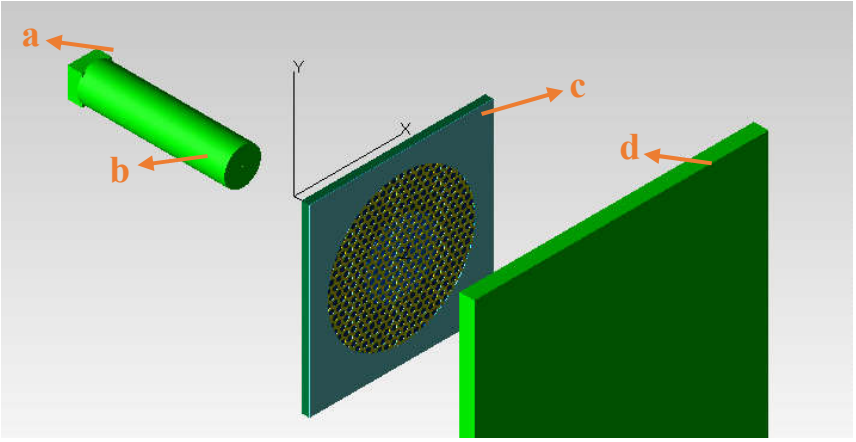

Figure 3.5. The simulation setup created for defining the optimum distance to the substrate

In Figure 3.5, the surface that is placed for collecting the flux returning to the fiber is shown as (a). The single mode fiber is modeled with 9 µm core diameter and 125 µm cladding and shown as (b). 3-D modeled MEMS microphone is shown as (c). The surface shown as (d) is used for collecting the flux is escaped from the MEMS microphone.

In Figure 3.6, the variation of the power ratio according to change of distance to back surface of the substrate is given. Since the power ratio values after 300 µm converges to 0, the results between 300 µm and 1 mm are not included to the Figure 3.6 for the sake of visibility of the graph. The power ratio considerably increases from 50 µm to 0 µm. For the substrate thickness of 50 µm, the power ratio reaches 32.36%. Also, the power ratio reaches 15.03% for the substrate thickness of 500 µm. The simulations are consistent when Figure 3.4 and Figure 3.6 are compared. For the 0 µm distance between back surface of the substrate and fiber tip, the power ratio values are the same for the substrate thickness of 50 µm and 500 µm. Hence, the fiber tip should be placed as close as possible to back surface of the substrate thickness in order to acquire maximum reflected optical power. However, the substrate thickness cannot be reduced

to 50 µm with post processing methods. In order to simulate the substrate thickness of under 500 µm, the "equivalent distance" concept is created. The concept is clearly explained in the next section.

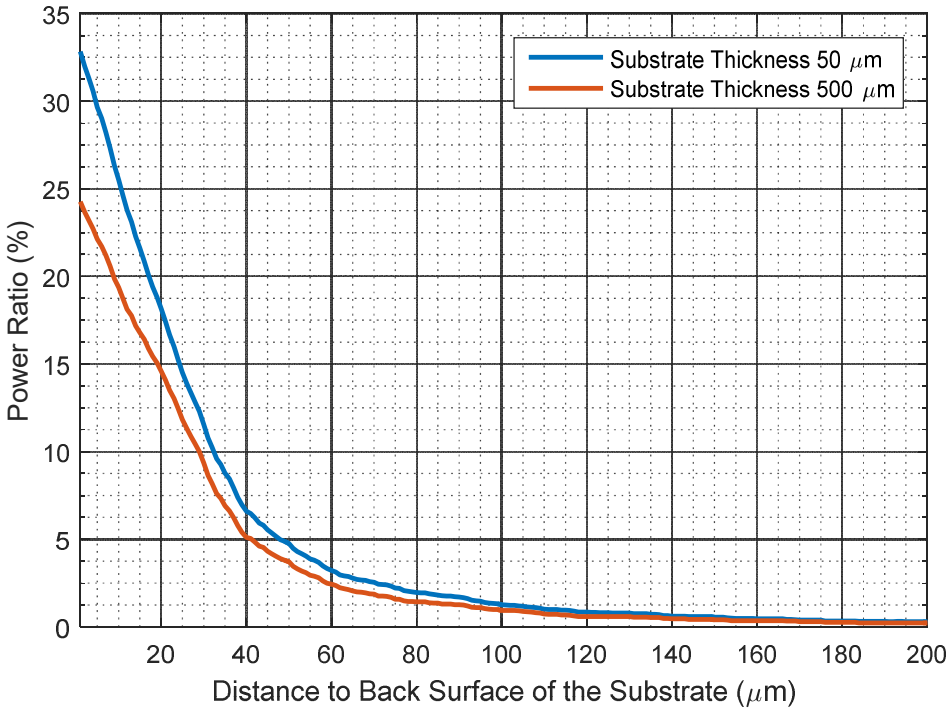

Figure 3.6. Distance to back surface of substrate vs. power ratio

3.4. Equivalent Distance Concept

The substrate thickness of the microphone cannot be decreased around the 50 µm with the grinding process. Since the grinding process applies a force on the chip and the chip becomes more fragile as the substrate thickness decreases, the chip is under the risk of being fractured and broken. Also, immobilization of the chip on the grinding table is hard because of the size of the chip being around 2 mm x 2 mm. Instead of grinding process, an alternative way of taking the similar measurement is needed.

The main purpose of the measurement is sensing the deflection of the diaphragm. Placing the fiber tip in front of the MEMS microphone is more convenient way of decreasing distance between the diaphragm and the fiber tip. The main purpose of the

concept is creating the same power ratio with different setup. By using such kind of topology shown in Figure 3.7, the diaphragm deflection is measured without preventing the movement of the diaphragm of the MEMS microphone. By varying the distance between the front surface of the MEMS microphone and the fiber tip, the equivalent power distance is searched. The desired distance is where the power ratio is around 32.36%.

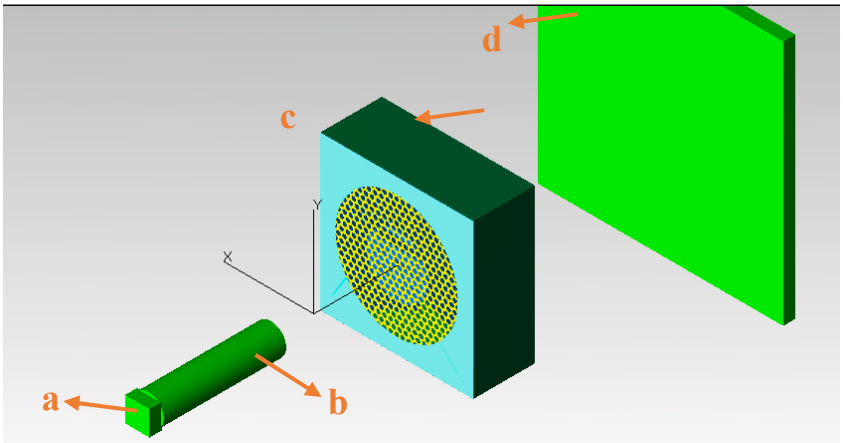

Figure 3.7. The simulation setup created for equivalent distance concept

The power obtained from the fiber tip - where the fiber tip is adjacent to the back surface of the MEMS microphone - is attempted to be equalized with the simulation setup shown in Figure 3.7. In Figure 3.7, the surface that is placed for collecting the flux returning to the fiber is shown as (a). The single mode fiber is modeled with 9 µm core diameter and 125 µm cladding and shown as (b). 3-D modeled MEMS microphone is shown as (c). The surface shown as (d) is used for collecting the flux is escaped from the MEMS microphone.

The simulation is run for the distance of 0 µm to 1000 µm. The power ratio is 32.36% where the substrate thickness is 50 µm. The power ratio of 32.4% is achievable at the distance of 28 µm which is derived from the Figure 3.8. Since the maximum deflection of the diaphragm is expected as order of 10 nm, the fiber tip does not affect the movement of the diaphragm from the distance of 28 µm. Hence, the measurement can

be taken without harming the measurement, deflection of the diaphragm and the MEMS microphone.

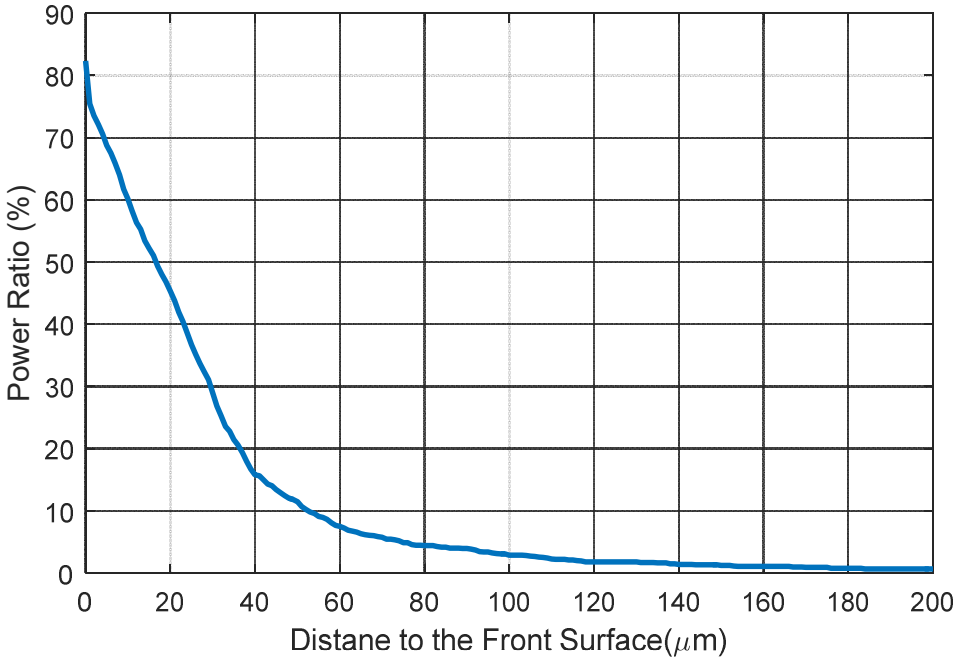

Figure 3.8. Distance to the front surface of the MEMS microphone vs. power ratio

CHAPTER 4

INSTALLATION OF THE MEASUREMENT SYSTEM

4.1. Construction of the Optical Part of the Measurement System

The optical part of the measurement system is constituted by laser diode, circulator, optical fiber, MEMS microphone and photodetector. The schematic of the optical part is shown in the Figure 4.1. Laser diode produces coherent light beams directed to the circulator. The circulator is responsible as separator for light beams incoming from laser diode and light beams outgoing to photodetector. The light beams passing through the optical fiber reaches the fiber tip and reflects from both fiber tip and MEMS microphone. The returning light beams are interfered in the optical fiber and they are directed to the photodetector via circulator. The working principle of the optical part of the measurement system is summarized. After conceptualizing the working principle of the system, the properties of the elements of the optical part gain importance for the sake of the system. Hence, the important properties and creation of the compatible system within itself are given in detail below.

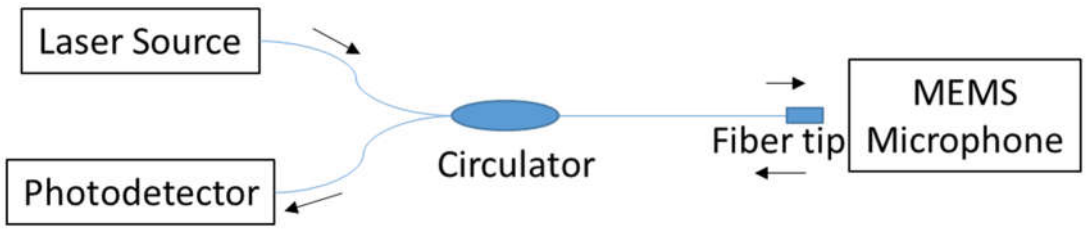

Figure 4.1. The schematic of the optical part of the measurement system

In order to illustrate more clearly, the details are given in flow of laser source to the photodetector. As a light source, a laser is used because the occurrence of the interference pattern requires the light beams that have same frequency or wavelength in the same medium. Hence, the intensity of the light is not distributed between

different wavelengths. As the span of the wavelength increases, the response of the photodetector to the light changes because of the photodetector having not flat responsivity. The more detailed explanation is given in below with the properties of the photodetector.

The working wavelength of the laser source is chosen as 1310 nm and laser power is kept at 100 mW. The MEMS microphone includes various layers based on Si and the substrate layer, which is the thickest layer of the MEMS microphone and is around 500 µm, the material of it is Si. The light beams which are sent and reflected back are passed through the substrate layer. Therefore, the photodetector receives the light beams which are exposed absorption twice by the substrate layer. Si has 95.9 cm^{-1} absorption coefficient at 980 nm and 2.7x 10^{-5} cm^{-1} absorption coefficient at 1310 nm as shown in Figure 4.2. Both wavelengths are common for laser sources. Therefore, wavelength of 1310 nm is chosen as the operating wavelength in order to minimally suffer from the attenuation due to the absorption in Si. The operating wavelength of the laser source also define the properties of the optical fibers and the circulator. They are included into the system according to the operating wavelength.

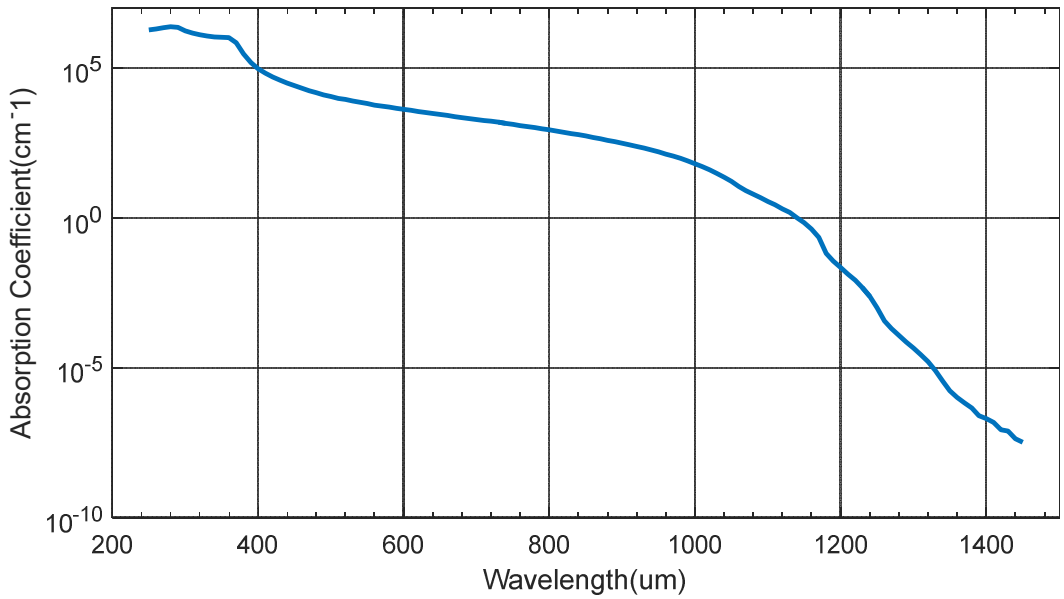

Figure 4.2. Absorption coefficient vs. wavelength graph for Si. Reproduced from [16].

Optical fibers and circulator are shown in Figure 4.3. Since the laser source with 1310 nm wavelength is available. It is chosen for the measurement system. In addition, the simulations are run at wavelength of 1310 nm.

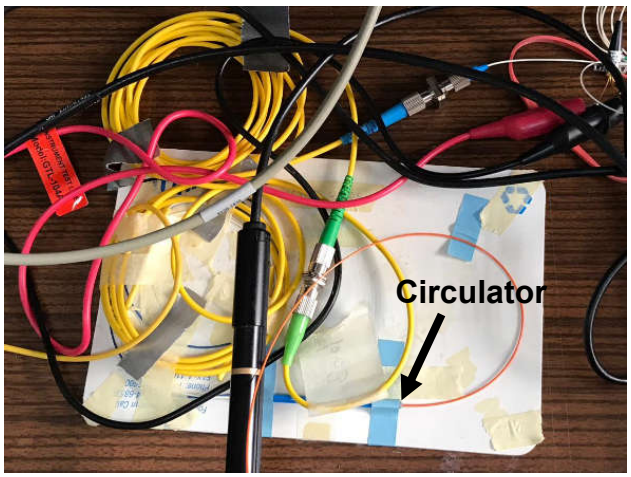

Figure 4.3. Optical fibers and circulator

The tip of the fiber is cleaved and mounted to the T-Cube DC Servo Controllers and 3 Z825B Motorized Actuators (ThorLabs, New Jersey, USA) which are shown in Figure 4.4. Each motorized actuator is connected to X, Y and Z tables in order to sensitive positioning of the fiber tip. The actuators have 29 nm positioning sensitivity and 25 mm travel length [17]. Since size of the diaphragm of the MEMS microphone is comparable to optical fiber thickness, sensitive positioning of the fiber tip is needed for alignment between the center of the diaphragm and the core of the optical fiber.

Figure 4.4. T-Cube DC Servo Controllers (left) and Z825B Motorized Actuators (right)

As stated in Section 2.1.2.1 Photodetector, Ge photodetector (ThorLabs PDA50B2) which is shown in Figure 4.5 is utilized for the sensing part of the measurement system. PDA50B2 is able to amplify and own eight position rotary switch which allows the user to vary the gain in 10 dB steps and designed for detection of light signals ranging from 800 to 1800 nm [18]. General specifications of the photodetector are given in *Table 4.1*. The returning fiber of the circulator is connected to the photodetector.

Figure 4.5. Ge photodetector

Table 4.1. *General specifications of Ge Detector [18]*

Active Area	Ø5.0 mm (19.6 mm^2)
Wavelength Range	800 to 1800 nm
Peak Wavelength	1550 nm (Typ.)
Peak Responsivity	0.85 A/W (Typ.)
Amplifier GBP	25 MHz
Max Output Current	100 mA
Gain Adjustment Range	0 dB to 70 dB
Output Voltage	0 to 5 V (50 Ω)

As stated in the Table *4.1*, the gain bandwidth of the preamplifier of the photodetector is 25 MHz. But, the bandwidth decreases while gain increases. During the measurement, the sensed signal can contain higher frequency components than

bandwidth because the bandwidth is dropped to 2 kHz at 50 dB gain. These components may not be sensed. Furthermore, collecting data for characterization at high frequencies is challenging without lock-in amplifier. In order to characterize the MEMS microphone at high frequencies, the lock-in amplifier (Stanford Research Systems SR850) is included into the measurement system. The use of the lock-in amplifier is explained in Section 4.2.

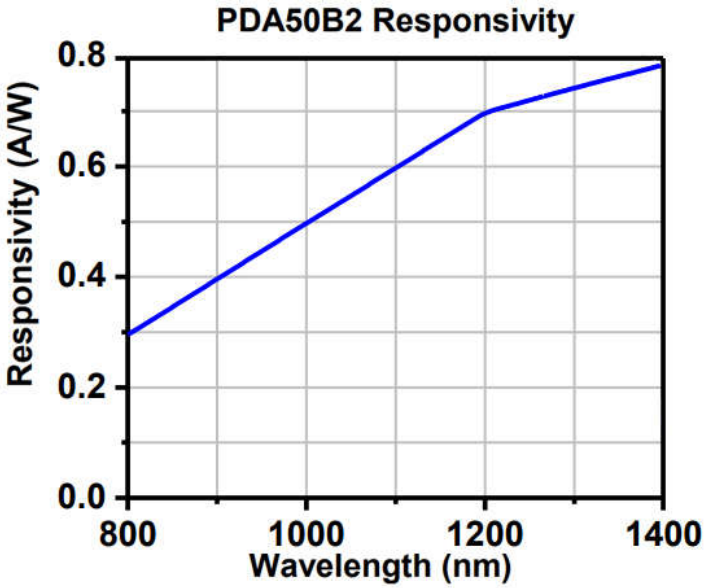

Figure 4.6. Responsivity graph of the Ge detector [18]

Operating wavelength also has advantage over 980 nm at photodetector side. In Figure 4.6, the responsivity graph of the detector is shown. While the responsivity at wavelength of 1310 nm is approximately 0.76 A/W, the responsivity at wavelength of 980 nm is 0.48 A/W. Use of 980 nm laser source with photodetector causes 37% loss in the sensed light intensity. Instead of suffering from attenuation and low responsivity, the operation at wavelength of 1310 nm provides optimal solution for the measurement system with low absorption and responsivity that is close to the peak responsivity. To sum up, the optical part of the system is mainly focused on obtaining

low attenuation, absorption and responsivity values that will not affect the measurement drastically, but feasible for construction of the whole system.

4.2. Construction of the Electrical Part of the Measurement System

The electrical part of the measurement system consists of a speaker, a waveform generator, a chip carrier and a lock-in amplifier. The speaker which is apart from its commercial examples is used for delivering high frequency (10 – 18 kHz) sound to MEMS microphone. It is driven by the driving circuit which takes signal inputs from Agilent 33220A Waveform Generator. The BNC cable having output from the waveform generator is connected to the driving circuit by solder.

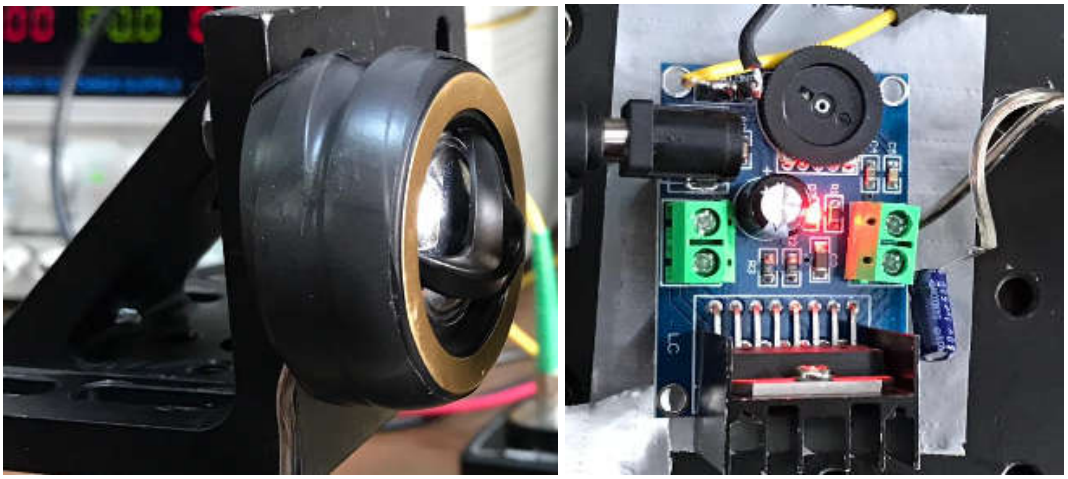

Figure 4.7. The speaker (left) and the driving circuit of the speaker (right)

The chip carrier is designed and produced in order to immobilize the MEMS microphone and apply bias to the chip. The chip is soldered on the chip carrier and the soldered part is grounded. Instead of BNC connectors, SMA type connectors are used to carry the bias. SMA connectors provide the chip with low series resistance with multiple lines of ground lines and multiple wirebonds. The chip is grounded from substrate, up, down, left and right pins. Carrying ground line from 4 different pads decreases noise stems from ground line of the measurement system. Also, there are 4 more pins on the chip allocated for application of bias. In Figure 4.8, pads for biasing are shown with (b) and ground pads are shown with (a).

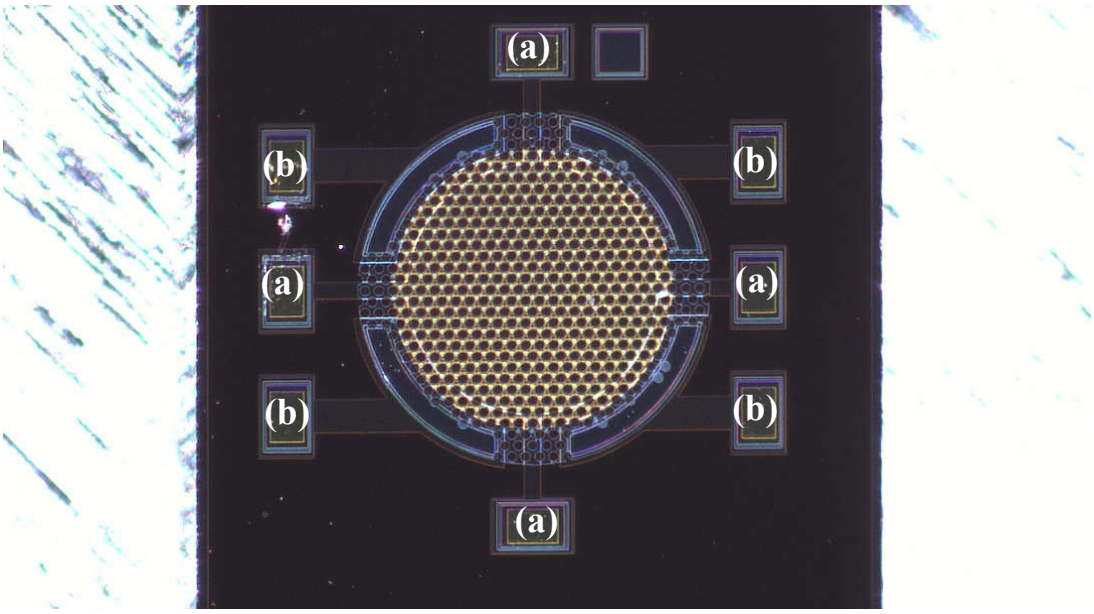

Figure 4.8. The chip under the microscope

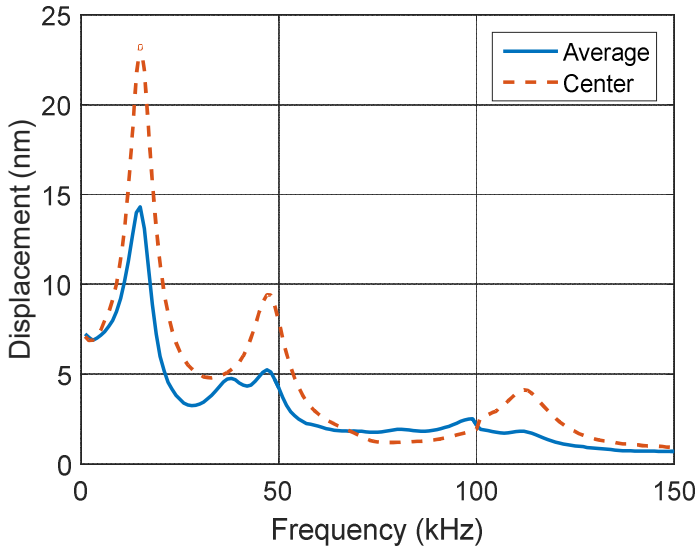

Figure 4.9. Laser vibrometer measurement of the chip

The characteristic of the chip is obtained via laser vibrometer measurement system. During the measurement, the membrane of the microphone is constantly excited and the displacement of the membrane is measured in various points. Since the center of the microphone is the most deflected part and fiber is focused to the center of the microphone, the center point data of the laser vibrometer measurement is presented.

The data is shown in Figure 4.9. *Laser vibrometer measurement of the chip*Figure 4.9. According to the data, the first resonant frequency of the membrane is 15 kHz. At the first resonant frequency, the displacement of the center of the membrane reaches its maximum value.

During calibration and experiment, the output of the photodetector is observed by an oscilloscope. The output is 0V to 5V analog signal. Oscilloscope is also used for the feature of Fast Fourier Transform (FFT) which helps to differentiate frequency components of the electrical signal. The incoming light beams creates interference pattern inside the core of the fiber. Thus, the light intensity is changing by the phase of the light. Since the phase difference between the light beams are dependent on change of acoustic pressure or waves, the output of the photodetector shows the change of the acoustic pressure. Thus, the frequency components of the applied sound waves are observed via FFT.

Although the gain of the photodetector can be increased to 70 dB, the bandwidth is not enough to observe the high frequency components. The gain is set at 30 dB for sufficient bandwidth which is 22 kHz [18]. In order to take more sensitive measurements, the lock-in amplifier (Stanford Research Systems SR850) which is shown in Figure 4.10 is included into the measurement system.

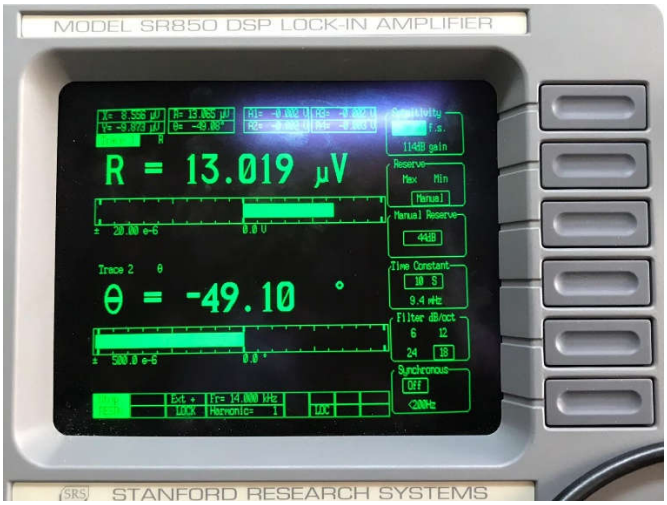

Figure 4.10. Stanford Research Systems SR850 lock-in amplifier

Figure 4.11. The MEMS microphone coupled to the chip carrier(left) and the cleaved fiber tip mounted on the XYZ stage(right)

In the Figure 4.11, the produced chip carrier is shown with (a). The MEMS microphone which is coupled to chip carrier is shown with (b). The label (c) shows the fiber mounted from the back of the chip carrier. The lock-in amplifier is used for characterization and taking sensitive and low noise measurements at high frequencies. Details of the measurements are explained in Section 4.3 The Complete Measurement System.

4.3. The Complete Measurement System

The measurement system is completed and run with the components stated above. In Figure 4.12, the schematic of the complete system is given. In Figure 4.13, the constructed measurement system is shown. The optical and electrical parts are assembled and the measurements are taken successfully.

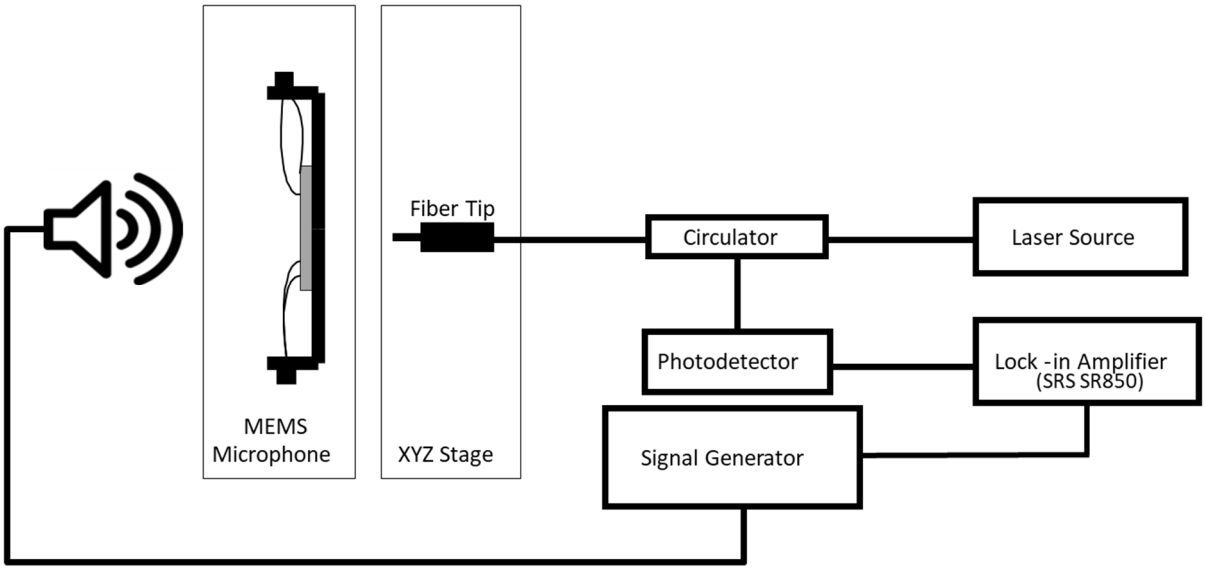

Figure 4.12. The schematic of the complete measurement system

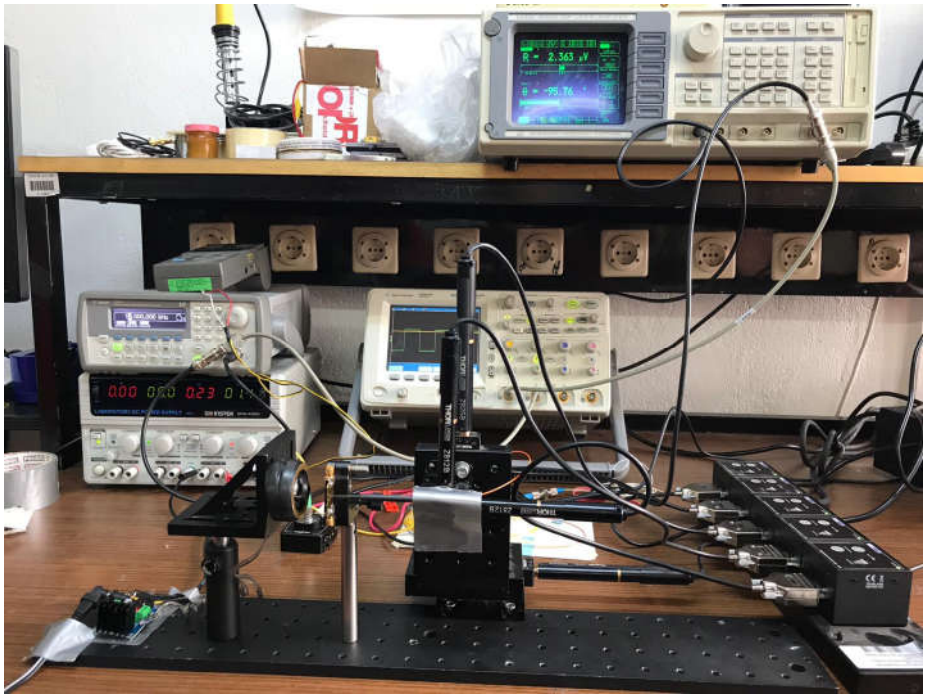

Figure 4.13. The overall measurement system

In Section 4.2, the purpose of the use of the lock-in amplifier is mentioned. In addition to being obliged to use the photodetector at low gain, the lock-in amplifier is used because of low SNR of the measurement system. The measurements are taken with 1

kHz steps from 2 kHz to 20 kHz. Due to the low responsivity of the speaker, valid data is not collected frequencies below the 2 kHz. Different method is used in order to excite the membrane of the microphone in wider range than 2 kHz to 20 kHz. The method is presented in the Section 4.3.2 Exciting Membrane by Applying Voltage. The various peaks are observed. Fluctuations and voltage drops may be related with decrease in coupling efficiency between the fiber tip and the MEMS microphone due to noise. Since the taken measurement is below the first resonant frequency of the microphone, a flat voltage response is expected. As shown in the Figure 4.14., the voltage response has fluctuations and the response is not flat. Possible noise types and sources are considered in Section 4.3.1 Noise Analysis.

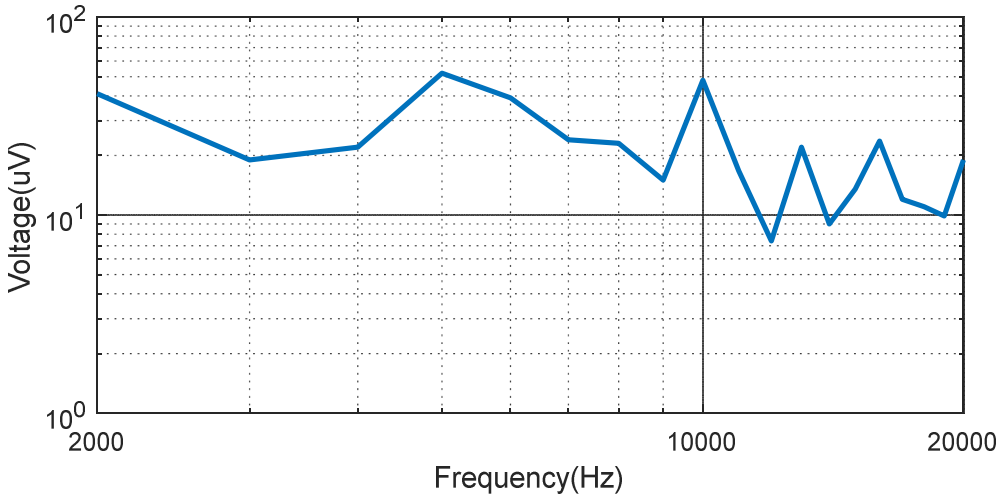

Figure 4.14. Voltage response of the MEMS microphone

4.3.1. Noise Analysis

When the measurement system is considered, there are two major sources of the noise. These are vibrational and electrical noises. The other noise parameters, such as photon noise, thermal noise, are not considered since their effect on the measurement is negligible. The noises due to electrical factors that can affect the system are electromagnetic interference because of using multiple measurement device close to each other, AC power line noise which can affect the ground level of the measurement devices and the fan noises of the measurement devices which introduces 60 Hz

vibrational noise to the measurement table. AC power line noise can affect the power or the measurement lines such as power line of the photodetector and the cable that carries signal from photodetector to lock-in amplifier. Since the shielded coaxial cable is used when carrying signal from photodetector to lock-in amplifier, AC power line noise is not considered as an important noise factor. Also, this is valid in the electromagnetic interference case because the signal carrying cables are either coxial or fiber optic cables. Vibrational noise due to components working with 60 Hz AC power line is created with multiple devices working with AC power line such as DC power source, signal generator, lock-in amplifier, PC, the power source of the photodetector and vacuum pump which is also placed in the laboratory. The effect of the vibrational sources is checked via carrying one of the devices to another table or shutting one of them down. The improvements in measurement stability and noise factors are observed.

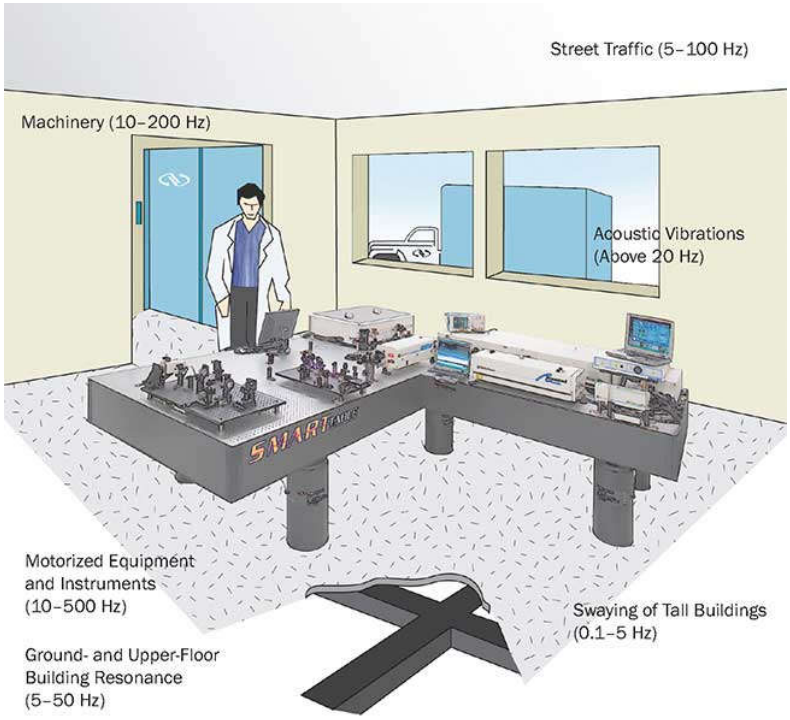

Figure 4.15 Various ambient vibration sources [32]

As shown in Figure 4.15, there are various vibrational noise sources that cannot be controlled and can affect the sake of the measurements. In Figure 4.11, the fiber tip is augmented towards the back of the chip carrier. Since the table which is used have metal legs and wooden desktop, it delivers vibrations created by measurement devices to the metal fixator and XYZ stage. The vibration proceeds through the fiber tip and its effect is amplified since the fiber tip is augmented. The MEMS microphone has 36 μm holes and membrane diameter of 1 mm which are susceptible to be misaligned with fiber tip. Although the chip carrier, which is shown in Figure 4.11, has hole in order to place the fiber tip which is augmented with telescopic carrier, it is not surely concluded that the vibrations at fiber tip are prevented. Therefore, the fixator of the fiber tip should be separated from the table.

The separator material should not have modes with natural frequencies at 50 and 60 Hz. Commercial isolation material which has modal analysis done have been searched. Polyurethane foam, which is used for isolation purposes on the building, is an easy to reach material. The modal analysis of the material shows appropriate properties for suppression of 60 Hz vibrational noise since 50 Hz and 60 Hz are not coinciding with natural frequencies listed below [33]. The modal analysis of the polyurethane foam is shown in Table 4.2.

Table 4.2 *The experimental natural frequencies for 36 mm polyurethane foam [33].*

Mode	36 mm Polyurethane Foam
	Natural Frequency (Hz)
1	42.59
2	54.21
3	69.43
4	78.52
5	88.56

The separator is produced and additional foam added on top of the polyurethane foam. The separator is placed under the chip carrier, fiber optic cable fixator and XYZ stage which is shown in the Figure 4.16 with orange color.

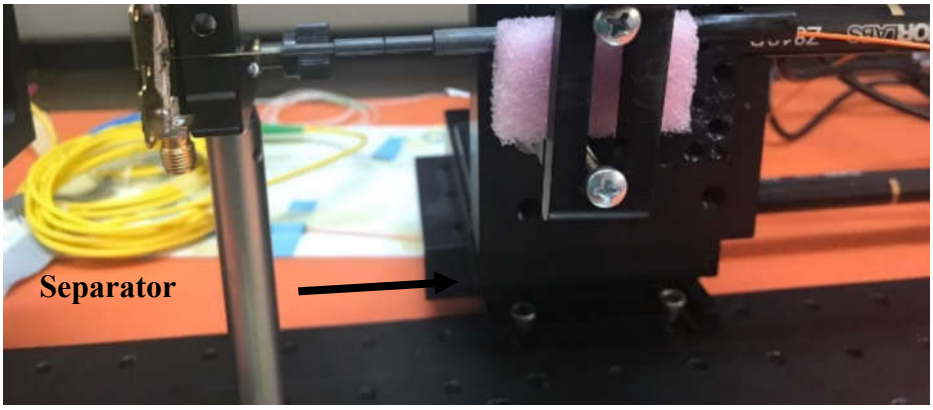

Figure 4.16 The separator placed under the chip carrier and XYZ stage

4.3.2. Exciting Membrane by Applying Voltage

The design of the MEMS microphone includes pads for applying bias to membrane. By applying bias to the microphone, the air gap distance can be changed. The behavior of the membrane changes with the type of applied bias. The membrane is fixated to the shorter air gap distance when only DC bias is applied. By applying combined AC and DC bias, air gap distance can be controlled and membrane can be excited with frequency of the AC bias. Experimentally excitation of the membrane is shown in Figure 4.17. In order to verify the applicability of the DC and AC bias to the MEMS microphone, 0.5V DC and 0.5Vpp AC bias with 6 different frequencies which are in the range of 10 kHz to 50 kHz is applied to the microphone which is shown in Figure 4.17. After the bias applied to the membrane, the fiber tip is placed close to the membrane in order to measure the deflection. Similar to the working principle of the optical measurement system, the fiber tip collects the reflected light and delivers to the photodetector. The photodetector converts light to electrical signals which is fed to the oscilloscope. The signal delivered by the photodetector is analyzed under FFT. The excited frequencies is verified by FFT results of the experiment.

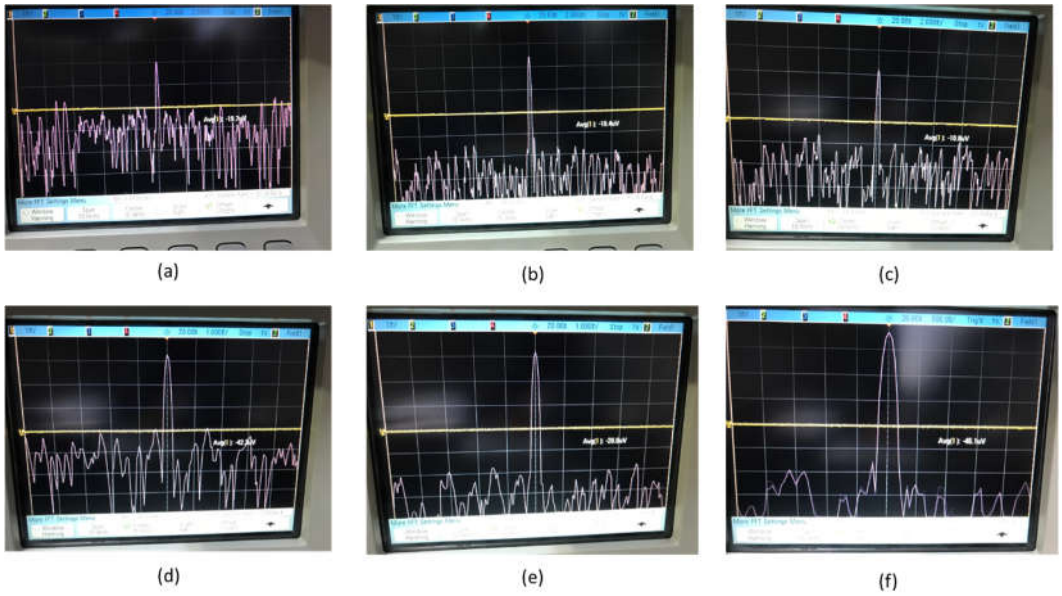

Figure 4.17 FFT measurements of excited membrane of the MEMS microphone with frequencies of 10 kHz (a), 15 kHz (b), 20 kHz (c), 25 kHz (d), 30 kHz (e) and 50 kHz (f)

Since the applicability of the AC and DC bias to the microphone is verifed, the measurement setup can be improved with external excitation of the membrane of the microphone. The speaker has non-flat response to the tones with different frequencies. It has gradually increasing sound level with increasing frequency which varies from 50 Hz to 10 kHz. After reaching its sound level peak, the sound level of the speaker decreases with the increasing frequency which varies from 10 kHz to 20 kHz. With adaptation of the excitation of the membrane by applying bias voltage, the characteristics of the microphone is evaluated without requirement of the characterization of the speaker. In order to characterize the microphone directly, DC and AC bias with constant amplitude and varying frequency is applied.

The differences between the measurement systems proposed in Figure 4.13 and Figure 4.18 are listed as follows:

- The separator is placed under the XYZ stage which holds the fiber tip with fixator
- The chip carrier is flipped. The top of the MEMS microphone is faced with the fiber tip.

- Signal generator is connected to the chip carrier instead of the speaker.

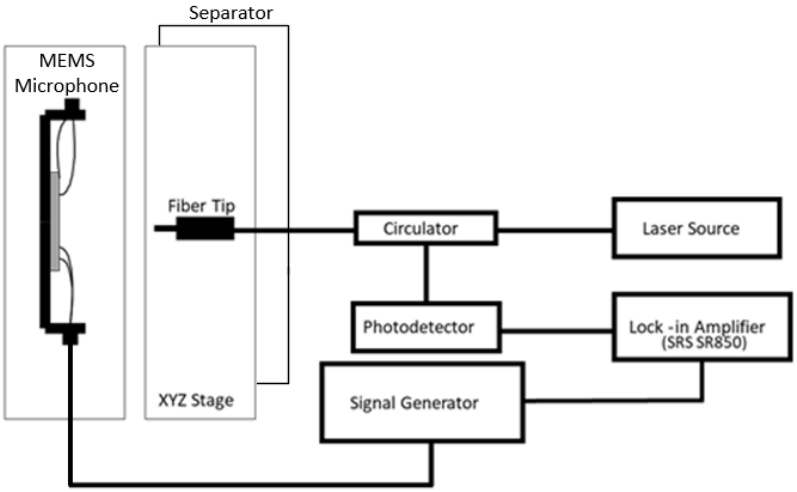

Figure 4.18 The measurement system with external membrane excitation

The measurement method is similar with the method defined as in the Section 3.4 Equivalent Distance Concept. In this configuration, the deflection of the membrane is measured instead of determining the equivalent distance required for desired power ratio.

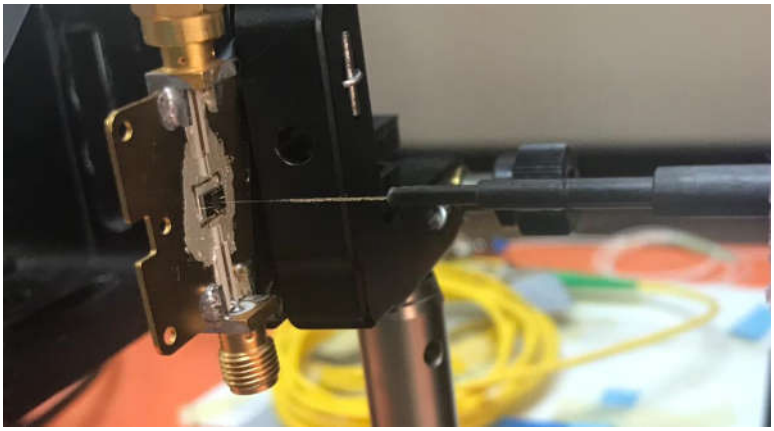

Figure 4.19 The chip carrier and the fiber tip modified for measurement with membrane excitation

The measurement is taken with 0.5V DC and 100 mV Vpp AC applied bias, frequency sweep range from 20 Hz to 20 kHz and 10 sec averaging time of lock-in amplifier. The noise floor measurement is taken as shown in Figure 4.20. The mean of the noise

floor is 235 nV and standard deviation of the noise floor 95 nV. The voltage response of the microphone is shown in Figure 4.20. The mean of the signal is 49.57 µV and standard deviation of the signal is 20 µV.

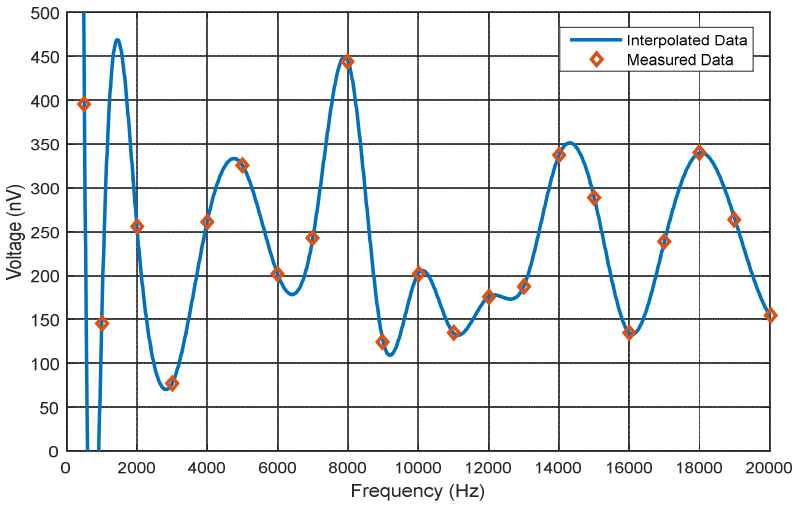

Figure 4.20 Noise floor vs. frequency measurement

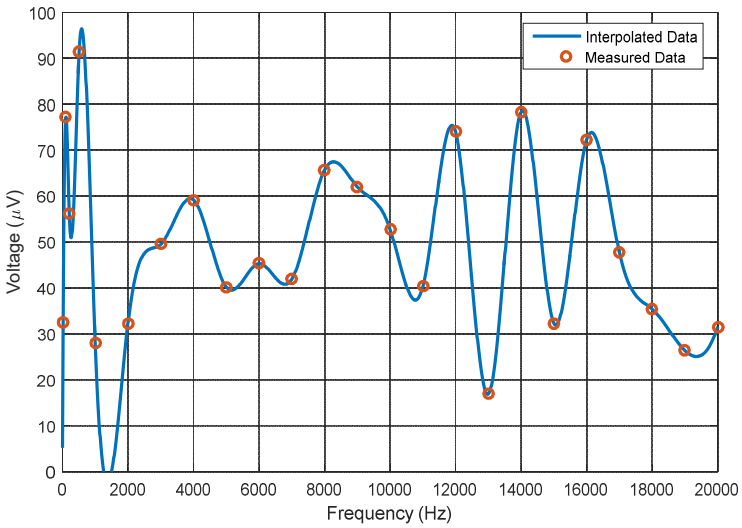

Figure 4.21 Voltage response of the microphone

With combining noise floor and voltage response of the microphone, signal to noise ratio which is shown in Figure 4.22 is derived. The signal to noise ratio has mean of 22.88 dB and standard deviation of 3 dB. The signal to noise ratio is relatively flat as

expected. In order to decrease the standard deviation of the signal to noise ratio, these experiments and measurements should be repeated on the optical table.

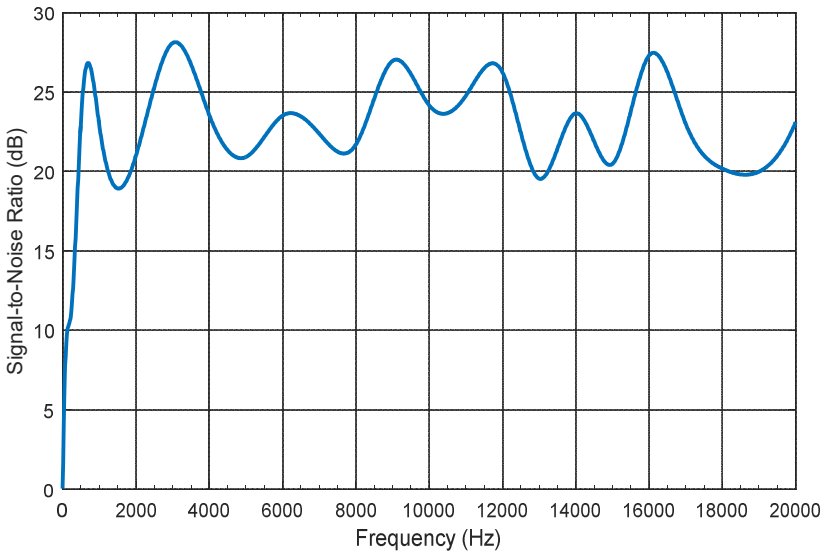

Figure 4.22 Signal to noise ratio vs. frequency graph of the microphone

4.3.3. Self Biasing

The light beams sent from the top of the MEMS microphone are also modulated while transmitting through the microphone. The reflected light is modulated due the membrane deflection and the light transmitted through the microphone is also modulated with 180° phase shift relative to reflected light. Since the transmitted light power gives information about the reflected light power, the voltage created due to the light incident on the photodetector can be used for biasing the microphone. After characterization of the microphone according to bias voltage amplitude and frequency, the additional photodetector can be used for feedback purposes. For the future work, it is expected to control the sensitivity of the microphone automatically and instantaneously. The schematic describing the operation is shown in Figure 4.23.

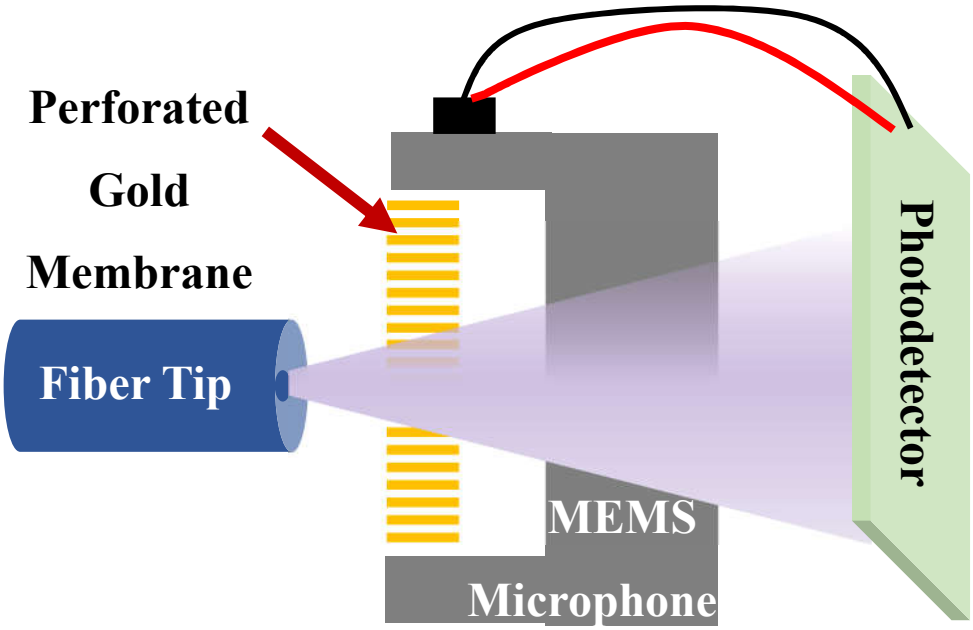

Figure 4.23 Schematic of the self biasing MEMS microphone

The measurements setup is shown in Figure 4.24. The MEMS microphone is biased with voltage generated by the photodetector. The voltage created on the photodetector is measured as 51.6 mV when the MEMS microphone is placed between photodetector and fiber tip. In this configuration, roughly 500 mV is created on the photodetector without the MEMS microphone. The loss is due to absorption in the substrate. The microphone can be self biased.

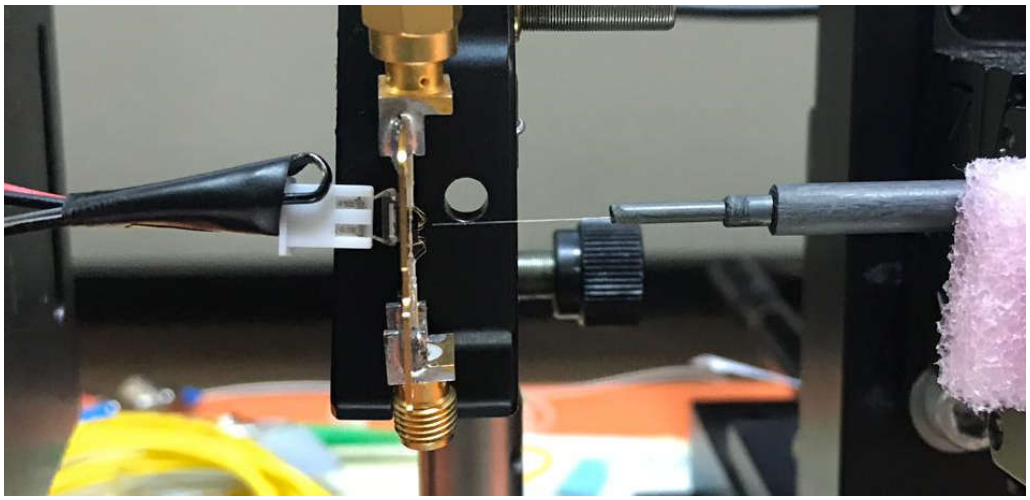

Figure 4.24 Self biasing MEMS microphone measurement setup

CHAPTER 5

CONCLUSION

The fiber optic MEMS microphone measurement system is designed, assembled and verified. The design of the system is based on construction of Fabry-Perot Interferometer. The Fabry-Perot Interferometer is constructed between the diaphragm coated with Au and tip of the cleaved fiber. Because sufficient power of light is not observed at the photodetector, the optimization of the system is required. In order to optimize the system, the simulations are run for examining and understanding the structure thoroughly.

Simulations are run at 3 different topologies. Each of them is constructed with different optimization purpose. They are constructed for optimizing the distance between substrate and fiber tip, substrate thickness and an alternative way of taking measurements with MEMS microphones. The consistency between the simulations are checked and the material properties supplied into the simulation according to operating wavelength.

The simulations run have shown that the substrate thickness and distance between substrate thickness and fiber tip should be decreased as much as possible. However, the reducing substrate thickness without harming the MEMS microphone is not viable with the post processing methods. In addition, the optimum distance between the fiber tip and the back of the substrate is evaluated as a parameter because the fiber tip and the MEMS microphone are not fused to each other.

Substrate thickness could not be reduced without harming the microphone. Therefore, matching the power ratio at lower substrate thicknesses is desired. Equivalent Distance Concept is created in order to examine the feasibility of an alternative way of measuring the diaphragm movement. The simulations show that the power ratio to be

obtained from substrate thickness of 50 μm is possible when the distance between the fiber tip and the front side of the MEMS microphone is set to 28 μm.

It is shown that evaluation of different substrate thicknesses is possible by this method, which will allow the estimation of the results of various combinations of existing diaphragm structures and substrate thicknesses. In addition to the different substrate thicknesses, the estimation of the behavior of the chip produced with different method is possible by implementing simulation parameters and 3D models belong to the designed chip. With this way, it is possible to evaluate whether the chips have the desired behavior before the production. Simulations shorten the design process while providing less time consumption due to shortening of test time, no need for procurement process and no need to wait for production periods. In addition, it is possible to eliminate production costs due to trial and error in compulsory cases.

The chip carrier is designed in order to take measurements safely and preserve the MEMS Microphone from environmental effects. The designed chip carrier is verified by the results. The results show that the desired bias voltage is successively applied to the MEMS Microphone and relatively low noise in the measurements are observed.

Furthermore, the measurement system is constructed with both optical and electrical components. The physical construction of the measurement system is given in detail. The elements, their working principles and compatibility between them are discussed. With the taken measurements, the functionality of the measurement system is verified with several measurements and relatively flat signal to noise ratio is obtained.

The measurement setup is modified in order to provide wider measurement range relative to measurements taken with speaker. The modifications give ability of exciting the membrane of the microphone externally to the measurement system. The modified measurement system is less susceptible to noise figures relative to unmodified measurement system. In addition, the separator is added into the measurement system to reduce the noise which stems from 50-60 Hz vibrations of the measurement equipment.

The self biasing MEMS microphone measurement system is also presented. The experiments related to the self biasing MEMS microphone provides encouraging results for creation of the system. With the realization of the system, the sensitivity of the microphone will be controlled optically. This control of the microphone may enable MEMS microphones being more adaptive to the pressure changes and maintaining high performance.

REFERENCES

[1] Lee, B., Kim, Y., Park, K., Eom, J., Kim, M., Rho, B. and Choi, H. (2012). Interferometric Fiber Optic Sensors. Sensors, 12(3), pp.2467-2486.

[2] Yang, S. and Xu, Q. (2017). A review on actuation and sensing techniques for MEMS-based microgrippers. Journal of Micro-Bio Robotics, 13(1-4), pp.1-14.

[3] Tanaka, M. (2007). An industrial and applied review of new MEMS devices features. Microelectronic Engineering, 84(5-8), pp.1341-1344.

[4] Huang, Y., Sai Sarathi Vasan, A., Doraiswami, R., Osterman, M. and Pecht, M. (2012). MEMS Reliability Review. IEEE Transactions on Device and Materials Reliability, 12(2), pp.482-493.

[5] Bogue, R. (2007). MEMS sensors: past, present and future. Sensor Review, 27(1), pp.7-13.

[6] Scheeper, P., van der Donk, A., Olthuis, W. and Bergveld, P. (1994). A review of silicon microphones. Sensors and Actuators A: Physical, 44(1), pp.1-11.

[7] Konle, H., Paschereit, C. and Röhle, I. (2009). A fiber-optical microphone based on a Fabry–Perot interferometer applied for thermo-acoustic measurements. Measurement Science and Technology, 21(1), p.015302.

[8] Hu, A., Cuomo, F. and Zuckerwar, A. (1992). Theoretical and experimental study of a fiber optic microphone. The Journal of the Acoustical Society of America, 91(5), pp.3049-3056.

[9] Bucaro, J., Lagakos, N., Houston, B., Jarzynski, J. and Zalalutdinov, M. (2005). Miniature, high performance, low-cost fiber optic microphone. The Journal of the Acoustical Society of America, 118(3), pp.1406-1413.

[10] En.wikipedia.org. (2019). Wave interference. [online] Available at: https://en.wikipedia.org/wiki/Wave_interference [Accessed 17 Apr. 2019].

[11] Wang, A., Xiao, H., Wang, J., Wang, Z., Zhao, W. and May, R. (2001). Self-calibrated interferometric-intensity-based optical fiber sensors. Journal of Lightwave Technology, 19(10), pp.1495-1501.

[12] Arndt, V., Müller, H. and Dopheide, D. (1996). Comparison measurements for selection of suitable photodetectors for use in Nd: YAG LDA systems. Experiments in Fluids, 20(6), pp.460-465.

[13] Eng, P., Song, S. and Ping, B. (2015). State-of-the-art photodetectors for optoelectronic integration at telecommunication wavelength. Nanophotonics, 4(3).

[14] Dutton, H. (1998). Understanding optical communications. Upper Saddle River (New Jersey): Prentice Hall.

[15] Fiber Optic Network Products. (2019). Single-mode Fiber vs. Multimode Fiber: Which to Choose?. [online] Available at: http://www.fiberopticshare.com/single-mode-fiber-vs-multimode-fiber-choose-2.html [Accessed 17 Apr. 2019].

[16] Green, M. (2008). Self-consistent optical parameters of intrinsic silicon at 300K including temperature coefficients. *Solar Energy Materials and Solar Cells*, 92(11), pp.1305-1310.

[17] Z8 Series Motorized DC Servo Actuators User Guide, ThorLabs.

[18] PDA50B2 Ge Switchable Gain Detector User Guide, ThorLabs.

[19] Keiser, G. (2015). Optical fiber communications. Singapore: McGraw Hill Education.

[20] Huang, D., Pintus, P., Zhang, C., Morton, P., Shoji, Y., Mizumoto, T. and Bowers, J. (2016). Dynamically reconfigurable integrated optical circulators. Optica, 4(1), p.23.

[21] Shah, M., Shah, I., Lee, D. and Hur, S. (2019). Design Approaches of MEMS Microphones for Enhanced Performance. Journal of Sensors, 2019, pp.1-26.

[22] Sessler, G. M. (1991). Acoustic sensors. Sensors and Actuators A: Physical, 26(1-3), 323–330. doi:10.1016/0924-4247(91)87011-q

[23] https://www.lambdares.com/tracepro/ [Accessed at 29.05.2019]

[24] http://www.laseoptics.com/Lensed-Tapered-Fibers-Description.pdf [Accessed at 17.09. 2019]

[25] Lin, S. (2005). A lensed fiber workstation based on the elastic polishing plate method. Precision Engineering, 29(2), 146-150. doi: 10.1016/j.precisioneng.2004.05.008

[26] Szu-Ming Yeh, Sun-Yuan Huang, & Wood-Hi Cheng. (2005). A new scheme of conical-wedge-shaped fiber endface for coupling between high-power laser diodes and single-mode fibers. Journal Of Lightwave Technology, 23(4), 1781-1786. doi: 10.1109/jlt.2005.844511

[27] Eun-Hyun Park, Moon-Jung Kim, & Young-Se Kwon. (1999). Microlens for efficient coupling between LED and optical fiber. IEEE Photonics Technology Letters, 11(4), 439–441. doi:10.1109/68.752541

[28] Cohen, L., & Schneider, M. (1974). Microlenses for Coupling Junction Lasers to Optical Fibers. Applied Optics, 13(1), 89. doi: 10.1364/ao.13.000089

[29] Thual, M., Rochard, P., Chanclou, P., & Quetel, L. (2008). Contribution to Research on Micro-Lensed Fibers for Modes Coupling. Fiber and Integrated Optics, 27(6), 532–541. doi:10.1080/01468030802272450

[30] https://www.thorlabs.com/newgrouppage9.cfm?objectgroup_id=358 [Accessed at 17.09. 2019]

[31] https://www.thorlabs.com/newgrouppage9.cfm?objectgroup_id=12000 [Accessed at 17.09.2019]

[32] Booth, Warren. (2010). How to determine your equipment needs. Laser Focus World. 46. 65-71.

[33] Investigation Thickness Effects of Polyurethane Foam Core Used in Sandwich Structures via Modal Analysis Method. (2017). May 22-24, 2017 Kuala Lumpur (Malaysia) ICLTET-2017, ACBES-2017. doi: 10.15242/iie.e0517006.

[34] http://www.highpak.com/fibre.html [Accessed at 18.09.2019]